frontiers | Frontiers in Earth Science

ORIGINAL RESEARCH
published: 27 April 2022
doi: 10.3389/feart.2022.866375

# Evolution of the Continental Crust in the Northern Tibetan Plateau: Constraints From Geochronology and Hf Isotopes of Detrital Zircons

*Zeyu Liu, Guibin Zhang*, Lu Xiong, Feng Chang and Shuaiqi Liu*

*The Key Laboratory of Orogenic Belts and Crustal Evolution, MOE, School of Earth and Space Sciences, Peking University, Beijing, China*

To investigate the evolution of the continental crust in the northern Tibetan Plateau, detrital zircon U–Pb geochronology and Hf isotopes analysis were performed on two fluvial sand samples from North Qaidam (the Yuka and Shaliu rivers). A total of 443 detrital zircon U–Pb ages and 244 Hf isotopic results were obtained and reveal that the South Qilian, North Qaidam, and East Kunlun terranes show affinity to the western Yangtze Block. Age distributions of detrital zircons from the Yuka River cluster mainly in two age intervals of 1,000–700 and 480–400 Ma. The corresponding $\varepsilon_{Hf}(t)$ values are mostly negative, with depleted two-stage Hf model ages ($T_{DM2}$) of 2.1–1.6 Ga. In contrast, age data for the Shaliu River fall in the ranges of 1,000–700, 460–380, and 260–200 Ma, with $T_{DM2}$ ages of 2.0–1.6 and 1.6–1.2 Ga. In addition, zircons with Neoproterozoic ages from both river samples possess common Paleoproterozoic $T_{DM2}$ ages (2.0–1.6 Ga, with a peak of 1.8–1.7 Ga), indicating that the South Qilian, North Qaidam and East Kunlun terranes were probably part of the same Neoproterozoic continent. The East Kunlun and North Qaidam terranes are inferred to include Mesoproterozoic continental crust (1.6–1.0 Ga), suggesting differences in crustal evolution between the East Kunlun–North Qaidam and Qilian terranes. Phanerozoic magmatism in these three terranes was sourced mainly from the recycling of ancient continental crust with minor contributions from the juvenile crust.

**Keywords: south qilian, north qaidam, east kunlun, detrital zircon, zircon U-Pb geochronology, hf isotopes**

OPEN ACCESS

***Edited by:***
*Michel Grégoire, Géosciences Environnement Toulouse (GET), France*

***Reviewed by:***
*Simon Johnson, Geological Survey of Western Australia, Australia*
*Oscar Laurent, Géosciences Environnement Toulouse (GET), France*

****Correspondence:***
*Guibin Zhang*
*gbzhang@pku.edu.cn*

***Specialty section:***
*This article was submitted to Petrology, a section of the journal Frontiers in Earth Science*

***Received:*** *31 January 2022*
***Accepted:*** *06 April 2022*
***Published:*** *27 April 2022*

***Citation:***
*Liu Z, Zhang G, Xiong L, Chang F and Liu S (2022) Evolution of the Continental Crust in the Northern Tibetan Plateau: Constraints From Geochronology and Hf Isotopes of Detrital Zircons. Front. Earth Sci. 10:866375. doi: 10.3389/feart.2022.866375*

## 1 INTRODUCTION

The northern Tibetan Plateau is an ideal place to understand plate collision, interactions of tectonic uplift and crustal evolution. Although Tibetan Plateau has been studied for decades, most studies focus on the Cenozoic tectonic uplift (Tapponnier et al., 2001; Yin et al., 2008; Clark et al., 2010; Rohrmann et al., 2012; Wang et al., 2014; Botsyun et al., 2019), while rarely studying the crustal evolution from Proterozoic to Paleozoic by using the detrital zircon in the northern Tibetan Plateau.

Zircon is one of the most robust accessory minerals with refractory nature during weathering and transportation, meaning that the U–Pb isotope system of detrital zircons can be used to obtain reliable chronological information, which in turn can be used to track the source region of the host clastic sedimentary rocks. Combined with the stable Lu–Hf isotope compositions, analysis of detrital zircons from modern river sediments can lead to a better understanding of the history of continental growth (Belousova et al., 2010; Kröner et al., 2014; Chen et al., 2015; Xu et al., 2016; Gong et al., 2017).

Thus, detrital zircons can be used to help establish the geological history of regions through which rivers flow, and may record information about the evolution of magmatism and metamorphism in these regions (Lease et al., 2007; Nie et al., 2012; Blayney et al., 2016; Song et al., 2019).

Numerous studies have used detrital zircon U–Pb ages and Hf isotopes to track the continental growth (e.g., Condie et al., 2005; Liu et al., 2008; Yang et al., 2009; Geng et al., 2011; Sun et al., 2012), although data are scarce for the area of the northern Tibetan Plateau investigated in this study. The North China block and the Yangtze block are two stable cratons adjacent to the northern Tibetan Plateau. It is generally considered that 2.9–2.4 Ga were the main periods of crustal growth in the North China Craton, but thermal events from the Mesoproterozoic to early Paleozoic are missing (Yang et al., 2009). The Yangtze Craton records two Precambrian periods of growth at 3.8–3.2 and 0.91–0.72 Ga, which are consistent with detrital zircon ages obtained from the South Qilian and North Qaidam terranes located on the northern Tibetan Plateau (Liu et al., 2008). Thus, the high degree of similarity of detrital zircon ages between the western Yangtze Craton and South Qilian–North Qaidam terranes reveals their close affinity. However, there have been insufficient studies of the overall crustal evolution of the South Qilian, North Qaidam, and East Kunlun terranes, which are key areas for understanding the tectonic evolution of the northern Tibetan Plateau.

The North Qaidam ultra-high pressure metamorphic (UHPM) belt has attracted considerable research attention regarding the evolution of the adjacent Qilian and East Kunlun orogenic belts (Zhang et al., 2008; Song et al., 2011, Song et al., 2019.; Liu et al., 2012; Gao and Zhang, 2017; Gong et al., 2017; Jian et al., 2020; Wu et al., 2020). Gao and Zhang, 2017 conducted zircon U–Pb dating of metapelite from Lüliangshan and Dulan in the North Qaidam UHPM belt and concluded that the North Qilian was an active continental margin, and the North Qaidam was a passive continental margin during the early Paleozoic; then the North Qaidam changed to be an active continental margin after the closure of ancient Qilian Ocean. Liu et al. (2012) conducted U–Pb isotope dating of detrital zircons from Cenozoic sediments in the Lulehe section and modern river sands in the North Qaidam, revealing a record of Rodinia supercontinent break-up, Pan-African regional metamorphism related to the subduction and collision in the Nouth Qaidam–South Qilian area. It is generally considered that multi-stage arc magmatism and continental-collision felsic intrusive magmatism occurred in the South Qilian, North Qaidam, and East Kunlun terranes from the Paleozoic to Triassic during subduction in the Proto-Tethys and Paleo-Tethys oceans. However, relationships among these three terranes during the Paleozoic–Mesozoic multiple Wilson cycles remain debated. Two popular tectonic models for the Paleozoic–Mesozoic tectonic configuration of the South Qilian, North Qaidam, and East Kunlun terranes follow: 1) the archipelago model, which proposes that the three terranes were separated from each other by ocean basins during the early Paleozoic and amalgamated during the mid-to-late Paleozoic (Kang et al., 2019; Zhang et al., 2020); and 2) the continuous continent model, in which during the early Paleozoic, the continuous "North Qaidam-South Qilian" terrane were sandwiched between the North Qilian arc to the north and the Kunlun arc to the south (Cheng et al., 2017; Gehrels et al., 2003; Song et al., 2013, 2014), or the continuous "North Qaidam–East Kunlun" terrane and Qilian Terrane were separated by the Qilian Ocean (Jian et al., 2020).

Here we present results of detrital zircon U–Pb ages, trace-elements, and Hf isotopes collected from sediments of the Yuka and Shaliu rivers on the northern Tibetan Plateau with the aim of tracking the crustal growth and tectonic evolution of the South Qilian, North Qaidam, and East Kunlun terranes, which the three terranes dominated by the Paleoproterozoic-Mesoproterozoic continental crust, and support the archipelago model during the early Paleozoic.

## 2 GEOLOGICAL SETTING AND SAMPLES

The Paleozoic North Qaidam UHPM belt lies between the Qaidam and South Qilian terranes in the northern margin of the Tibetan Plateau (**Figures 1A–C**). It extends northwestward from Dulan, through Xitieshan and Lüliangshan, to Yuka over an overall length of ~400 km (**Figure 1D**). From the Neoproterozoic to the middle Permian, tectonic–thermal activities in North Qaidam were very intense (Li et al., 1999; Wu, 2008). The intense Neoproterozoic magmatic activity was most likely associated with the assemble and subsequent break-up of the Rodinia supercontinent, whereas the Paleozoic magmatic activity was probably related to the transition of the North Qaidam UHP belt from oceanic subduction to a continental collision regime (Wu et al., 2004; Song et al., 2009b; Zhang et al., 2013). Along the North Qaidam UHPM belt, eclogites are found as NW–SE-oriented boudins and interlayers within para- and orthogneisses in several localities (e.g., Dulan, Xitieshan, and Yuka) and garnet peridotite crops out in the Lüliangshan area (Song et al., 2009b; Zhang et al., 2013). The early stage of eclogite-facies metamorphism was at 473–443 Ma, representing the early oceanic subduction; then followed the continental deep subduction at 426–420 Ma. The reconstruction of Shaliuhe relict oceanic lithology provides evidence for oceanic subduction in the North Qaidam UHPM belt (Song et al., 2003, 2006, 2009a; Zhang et al., 2005, Zhang et al., 2008, 2009; Zhang and Zhang, 2011). Both coesite and diamond inclusions were found from eclogite, garnet peridotite, and country gneisses (Zhang et al., 2016 and references therein).

Dulan is located in the southeastern North Qaidam UHPM belt–northern Kunlun, which is located at the intersection of the South Qilian belt to the north, the East Kunlun Orogenic belt to the south-southeastward, and the Qinling to the east. The Dulan area was affected by multiple orogenic events during the Paleozoic–early Mesozoic, accompanied by tectonic–magmatic activities and granite intrusions. Three stages of Paleozoic granitic magmatism in Dulan had been identified, with S-type affinity: 434–432, 407–397, and 383–373 Ma (Yu et al., 2011), in which the early stage at 434–432 Ma formed more or less simultaneously with the North Qaidam HP/UHP metamorphism responded to

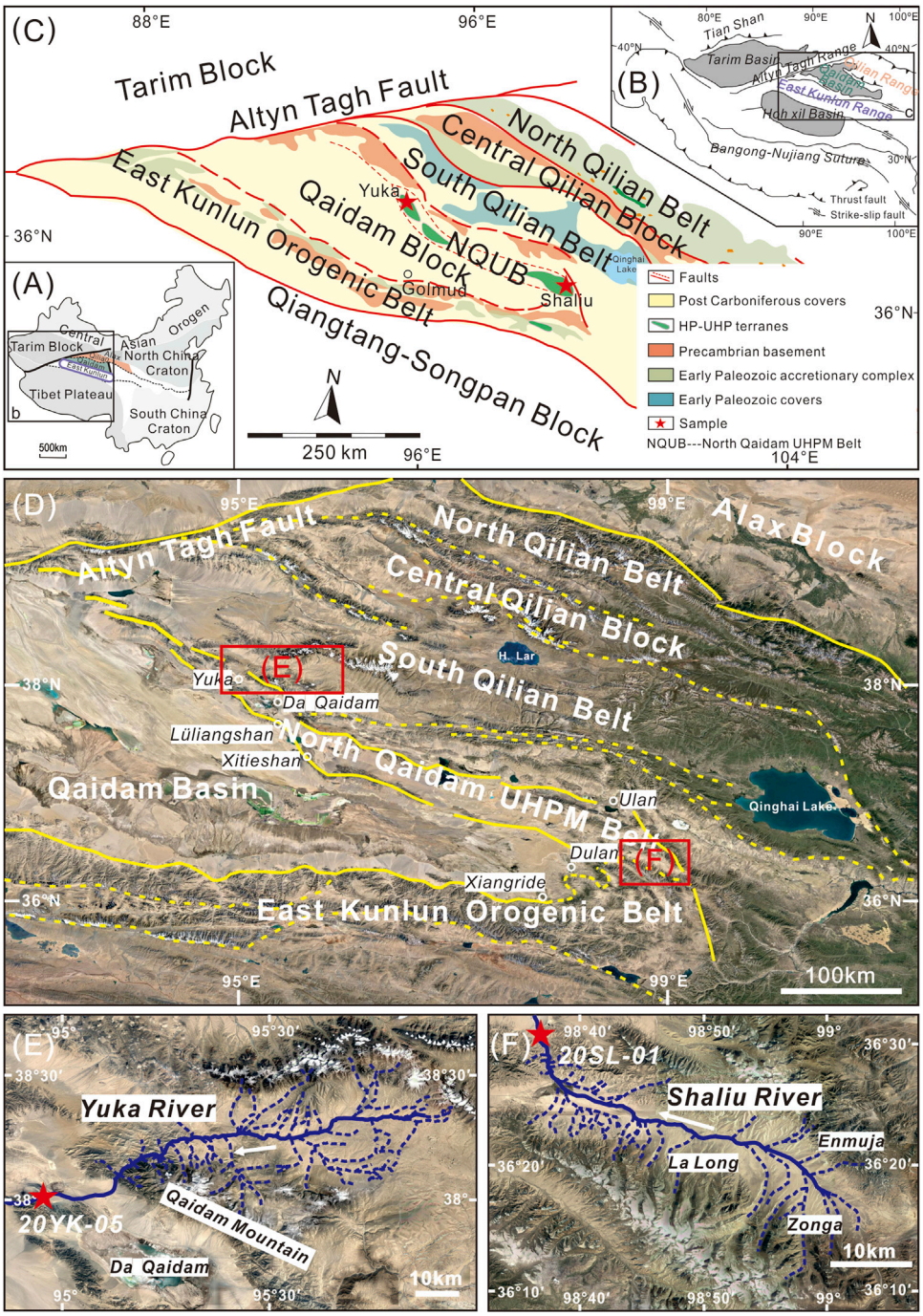


**FIGURE 1 | (A)** Location of the Tibetan Plateau within China; **(B)** Location of the Qilian Range, Qaidam Basin, and East Kunlun Orogenic Belt in the northern Tibetan Plateau (modified from Yin et al., 2008); **(C)** Simplified geologic maps of the northern Tibetan Plateau (modified from Song et al., 2018); **(D)** Satellite image of the study area showing the two sampling locations; **(E)** Close up view of the catchment area of the Yuka river and sample location of 20YK-05 (red star); **(F)** Close up view of the catchment area of the Shaliu river and sample location of 20SL-01 (red star).

the continental deep subduction and collision (Song et al., 2009b). While the others at 407–397 and 383–373 Ma may have been formed in association with break-off and exhumation of the subducted South Qilian slab and delamination of the lithospheric mantle, respectively (Yu et al., 2011). In addition, the Yematan granitoid represents an event spanning ~30 Myr, ranging from granodiorite with I-type affinities and biotite monzogranite (386–379 Ma), porphyritic biotite granite (367 ± 3 Ma), to diorite (374–360 Ma) (Wu et al., 2007; Wang et al., 2014). Post-collisional magmatic rocks in Dulan occurred

~20–30 Myr later than peak UHP metamorphism (ca. 420 Ma) of continental collision are highly diverse in age and composition, indicating multiple stages of magmatism, melting of various magma sources, and variable degrees of interaction between crust and mantle associated with a complex tectonic evolution from exhumation to orogenic collapse (Wang et al., 2014). Moreover, late Permian–Triassic granites are widely distributed in the eastern part of East Kunlun Terrane (Yuan et al., 2000). Late Triassic granites are widely developed in east of Dulan–Xiangride (Kui et al., 2010).

The Yuka area is part of the North Qaidam UHPM belt and is located between the South Qilian Terrane and the Qaidam Basin. Intermediate–felsic intrusive rocks are widely exposed in the Yuka area, and granites accompanied by UHP metamorphic rocks are well developed. Magmatic rocks are voluminous and represent multiple events, with more intense magmatism during the Caledonian event (early Paleozoic, at about 600–405 Ma) compared with Hercynian (late Paleozoic, at about 386–257 Ma) and Indosinian events (early Mesozoic, at about 257–205 Ma). The largest Paleozoic granite intrusion in the Yuka area is the Qaidamshan pluton, which is composed mainly of porphyritic monzonitic granite, granite porphyry, and granodiorite (He et al., 2020). The crystallization age of the Qaidamshan pluton was early Silurian–early Devonian (ca. 440–400 Ma), formed during continental collision (Wu et al., 2001; Lu et al., 2007; Wu, 2008).

Samples of modern river sediments collected during this study were obtained from the Yuka and Shaliu rivers. Sample 19YK-05 was taken from the Yuka River (**Figure 1E**), at a point located northwest of Dachaidan, west of the Qaidam mountains (38°0.2998′N, 94°56.8398′E). Sample 19SL-01 was taken from the Shaliu River (**Figure 1F**), at a point located in northeastern Dulan County, next to the G109 National Highway (36°31.2211′N, 98°36.6588′E).

## 3 ANALYTICAL METHODS

Zircon grains were separated using magnetic and heavy-liquid separation techniques and then handpicked under a binocular microscope. Zircon grains were set in an epoxy mount and polished to half thickness. Cathodoluminescence (CL) images were conducted with a Quanta 200F scanning electron microprobe (SEM) at the Key Laboratory of Orogenic Belts and Crustal Evolution, Ministry of Education, School of Earth and Space Sciences (SESS), Peking University (PKU), Beijing, China with conditions of 15 kV and 120 nA.

Zircon U–Pb geochronological and trace-element analyses were performed using a ThermoFisher iCapRQ ICP-MS coupled with a 193 nm GeoLas laser system at the SESS, PKU. The operating conditions are a laser spot diameter of 32 μm, a laser fluence of 5 J $cm^{-2}$, and a repetition rate of 5 Hz. The aerosol produced by ablation was carried by helium (0.70 L/min) mixed with argon and a small amount of nitrogen (each gas purity is >99.999%). Data reduction was conducted using Iolite software (Paton et al., 2011). Zircon 91,500 was used as an external standard, while GJ-1 and Plešovice were utilized as unknowns to monitor the precision and accuracy of U–Pb dating. Analysis of GJ-1 and Plešovice zircon standards yielded Concordia ages of 599.2 ± 1.2 Ma (2σ, n = 35, MSWD = 2.1) and 337.5 ± 0.7 Ma (2σ, n = 31, MSWD = 0.12), consistent with the recommended values reported in Jackson et al. (2004) and Sláma et al. (2008). The adopted U–Pb ages were $^{206}Pb/^{238}U$ ages for zircon grains with ages of ≤1.0 Ga and $^{207}Pb/^{206}Pb$ ages for grains with ages of >1.0 Ga. Ages with degrees of discordance of >10% were excluded from age calculations. Concordia diagrams were plotted using Isoplot 4.15 (Ludwig, 2003). Trace-element contents were analyzed from the same ablation crater as U-Pb dating and calibrated by $^{29}Si$ and NIST SRM 610, while NIST SRM 612 was used as a secondary standard (Pearce et al., 1997). Accuracy and precision were better than 5% for most elements. Analytical results for zircon dating and trace-element contents are presented in **Supplementary Tables S1. S2**. Analytical results for standard zircon dating are presented in **Supplementary Table S4**.

*In-situ* zircon Lu–Hf analyses were conducted using a Nu Plasma II MC–ICPMS coupled with a 193 nm GeoLas laser system at SESS, PKU. Analyses were performed with a laser energy of 8 J $cm^{-2}$, a repetition rate of 5 Hz, a spot diameter of 44 μm, and helium carry gas (0.63 L/min). Laser spots were positioned to half overlap or lie as close as possible to domains used for zircon U–Pb dating. Zircon 91,500 was analyzed as a calibration standard, and Plešovice and Penglai were adopted as secondary standards to monitor analytical quality. Data reduction was performed using Iolite software (Paton et al., 2011). Mass-dependent fractionation of Hf was corrected by internal normalization relative to a $^{179}Hf/^{177}Hf = 0.73250$ (Patchett and Tatsumoto, 1980) and Yb fractionation was corrected using the constant $^{173}Yb/^{172}Yb = 0.73925$ (Vervoort et al., 2004) and an exponential law. The isobaric interferences of $^{176}Lu$ and $^{176}Yb$ on $^{176}Hf$ were corrected by measuring the intensity of the interference-free $^{175}Lu$ and $^{172}Yb$ isotopes with the recommended $^{176}Yb/^{172}Yb$ ratio of 0.5887 and $^{176}Lu/^{175}Lu$ ratio of 0.02655 and assuming the fractionation factor $\beta_{Lu} = \beta_{Yb}$ (Vervoort et al., 2004). The analytical values of $^{176}Hf/^{177}Hf$ for the standard zircons were 0.282307 ± 0.000065 (2σ, n = 24) for 91,500, 0.282482 ± 0.000037 (2σ, n = 22) for Plešovice, and 0.282925 ± 0.000062 (2σ, n = 21) for Penglai, consistent with recommended values reported by Wu et al. (2006), Sláma et al. (2008), and Li et al. (2010), respectively. Present-day chondrite $^{176}Lu/^{177}Lu$ ratio of 0.0332 and $^{176}Hf/^{177}Hf$ ratio of 0.282772 (Blichert-Toft et al., 1997), and present-day depleted mantle values of $(^{176}Lu/^{177}Hf)_{DM} = 0.0384$ and $(^{176}Hf/^{177}Hf)_{DM} = 0.28325$ (Griffin et al., 2000) were used for the calculation of $\varepsilon_{Hf}$ (t) values and two-stage Hf model ages ($T_{DM2}$), respectively. Data for Lu–Hf isotopes of the samples and standard zircons are listed in **Supplementary Tables S3, S5**, respectively.

## 4 RESULTS

### 4.1 Detrital Zircon U–Pb Dating and Trace-Element Contents

CL images show that most zircons (>99%) have well-developed oscillatory zoning (**Figure 2**), suggesting a magmatic origin

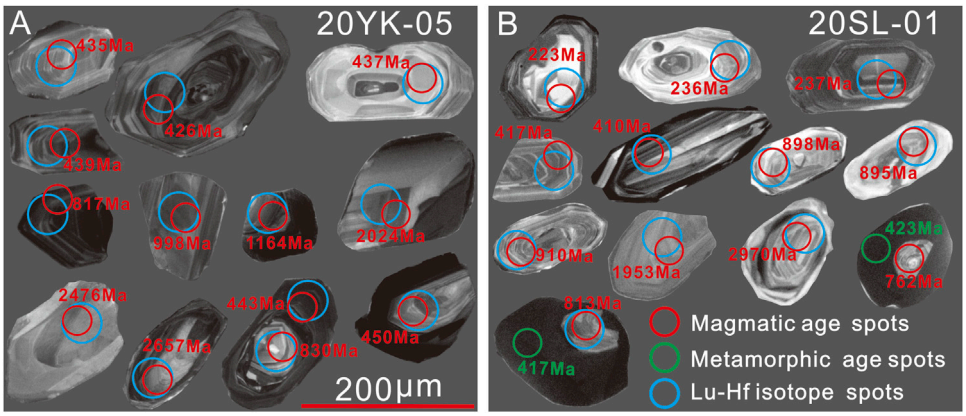


**FIGURE 2 |** Representative cathodoluminescence (CL) images for detrital zircon crystals of Sample 20YK-05 **(A)** and Sample 20SL-01 **(B)** from North Qaidam.

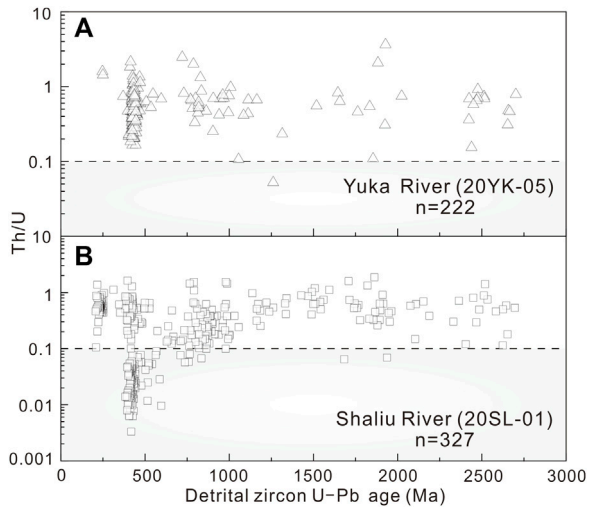


**FIGURE 3 |** Plot of Th/U ratios versus U-Pb ages of detrital zircons from the river sands of Sample 20YK-05 **(A)** and Sample 20SL-01 **(B)** from North Qaidam.

(Hoskin and Black, 2000; Corfu et al., 2003). Plots of Th/U versus U–Pb ages of detrital zircons and U–Pb age cumulative probability distributions for each sample are presented in **Figures 3**, **5A,B**, respectively.

On the basis of the substitution of ($REE^{3+}$ + $Y^{3+}$) for Zr in zircon from S-type granites being charge-balanced by $P^{5+}$, leading to a near 1:1 correlation between (REE + Y) and P, thus plots of (REE + Y) versus molar P can be used to distinguish the S-type and I-type zircons (Burnham and Berry., 2017; Zhu et al., 2020). Applying this classification method (S-type granites, i.e., 0.77*P< [REE + Y] <1.23*P for zircons with molar P > 15 μmol/g) to those zircons from the two samples with degrees of discordance of <10% shows that S-type granite zircons account for the majority (56.3%) of the Yuka River detrital zircons (**Figure 4A**), whereas I-type granite zircons account for the majority (73.8%) of the Shaliu River detrital zircons (**Figure 4B**). U–Pb age cumulative probability distributions and U–Pb Concordia diagrams for each age peak of S- and I-type zircons of the two samples are shown in **Figures 5C**,D, **6**. Selected detrital zircons with representative age peaks and mean values of age are given in **Supplementary Table S2**, and chondrite-normalized REE patterns are presented in **Figure 7**.

Zircons from the Yuka river (20YK-05) are characterized by oscillatory zoning textures and high Th/U ratio (mostly >0.1) (**Figures 2A**, **3A**), indicating a magmatic origin (Belousova et al., 2002; Corfu et al., 2003; Hoskin and Black, 2000; Rubatto, 2002). Some grains display core–rim zonation, with an oscillatory-zoned core and an un-zoned or oscillatory-zoned rim in CL images (**Figure 2A**). Of the 258 analyzed detrital zircon U–Pb ages from the Yuka River sample, 86.0% are concordant. Of these analyses, only one has Th/U ratio of <0.10 (0.05, 1,261 Ma), but it has likely a magmatic origin, as inferred from the oscillatory zoning texture. Detrital zircon U–Pb ages obtained for this sample cluster into two main ranges at 1,000–700 Ma and 480–400 Ma with peaks centering at 820 and 433 Ma, and two secondary ranges at 2800–2400 Ma and 2,100–1,500 Ma, respectively (**Figure 5A**). Compositionally, S-type zircon dominates ages of 460–402 Ma (**Figure 6A**), whereas I-type zircon dominates ages of 961–720 Ma and 472–412 Ma (**Figures 6B,C**). REE contents of sample 20YK-05 shows that S-type zircon has stronger negative Eu and Ce anomalies relative to I-type (**Figure 7A**), consistent with the known REE patterns of typical S- and I-type zircons (Burnham and Berry, 2017; Zhu et al., 2020).

Most analyzed zircons from the Shaliu river (20SL-01) are characterized by oscillatory zoning textures (Hoskin and Black, 2000; Corfu et al., 2003). About one-third of the analyzed grains have core–rim structures, with a core of oscillatory zoning and an un-zoned rim in CL images (**Figure 2B**), with Th/U ratios range of 0.01–1.87 (**Figure 3B**). Of the 336 detrital zircon U–Pb ages from the Shaliu River, 93.8% are concordant, with 223 data points are of magmatic origin and 92 data points are of metamorphic origin which distinguished by Th/U < 0.10 and un-zoned CL images; and three main ranges at 1,000–700 Ma, 460–380 Ma, and 260–200 Ma with peaks centering at 870 Ma, 420 Ma, and

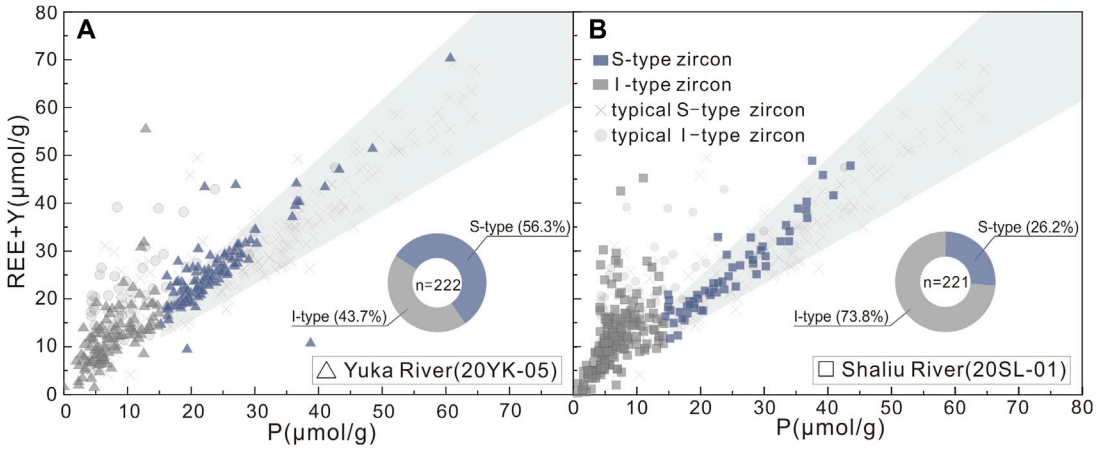


**FIGURE 4 |** Binary plot of molar *p* concentrations versus (REE + Y) for zircons of Sample 20YK-05 **(A)** and Sample 20SL-01 **(B)**. The gray-shaded area shows the field used to define zircon derived from S-type granites, i.e., 0.77**p*< (REE + Y) <1.23**p* for zircons with molar *p* > 15 μmol/g. The typical S and I-type zircon are collected from Burnham and Berry (2017) and Zhu et al. (2020).

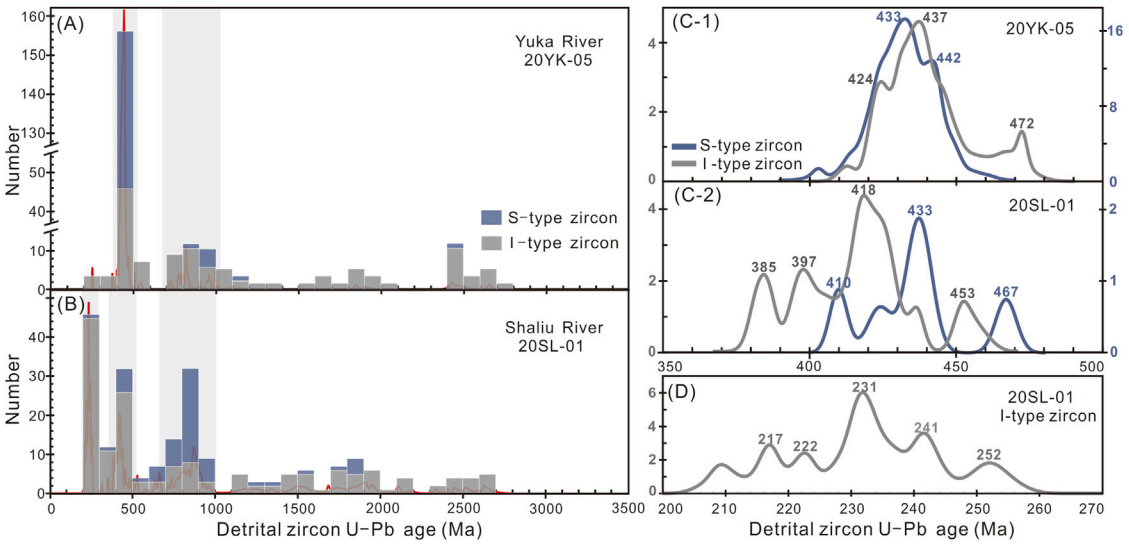


**FIGURE 5 | (A)** Histograms of detrital zircon U-Pb ages of sample 20YK-05, **(B)** Histograms of detrital zircon U-Pb ages of sample 20SL-01, **(C)** Relative probability plot for Early Paleozoic dates, **(D)** Relative probability plot for Late Paleozoic - Early Mesozoic dates.

232 Ma, and three secondary ranges at 2700–2300 Ma, 2000–1700 Ma, and 1,600–1,100 Ma, respectively (**Figure 5B**). With respect to composition, S-type zircon dominates ages of 915–776 Ma (**Figure 6D**), whereas I-type zircon dominates ages of 927–775 Ma, 458–381 Ma, and 256–207 Ma (**Figures 6E–G**). After excluding 16 mixed ages, the vast majority of the remaining 76 metamorphic zircons fall within the range of 456–383 Ma (**Figure 6H**). Analysis of REE contents for sample 20SL-01 shows the same characteristics as 20YK-05. Metamorphic zircons display flat HREE patterns with weak negative Eu anomalies (**Figure 7B**).

## 4.2 Lu–Hf Isotopes

Results of 224 Hf isotopic determinations are presented in **Supplementary Table S3** and **Figure 8**. **Figure 9** shows the distribution of $T_{DM2}$ ages (Wu et al., 2007; Yang et al., 2009).

Zircons from sample 20YK-05 (117 analyses) yield $\varepsilon_{Hf}$ (t) values of −29.1–16.2 (**Figure 8A**), and $T_{DM2}$ ages in the range of 3.8–1.3 Ga (**Figures 9A-1**), with a peak at 2.1–1.7 Ga. Zircon crystals with U–Pb ages of >1,000 Ma yield values of $\varepsilon_{Hf}$ (t) in the range of −12.8–16.2 (**Figure 8A**) and $T_{DM2}$ ages varying from 3.8 to 1.8 Ga (**Figures 9A-2**). Zircons in the age range of 1,000–700 Ma yield $\varepsilon_{Hf}$ (t) in the range of −17.1–2.3

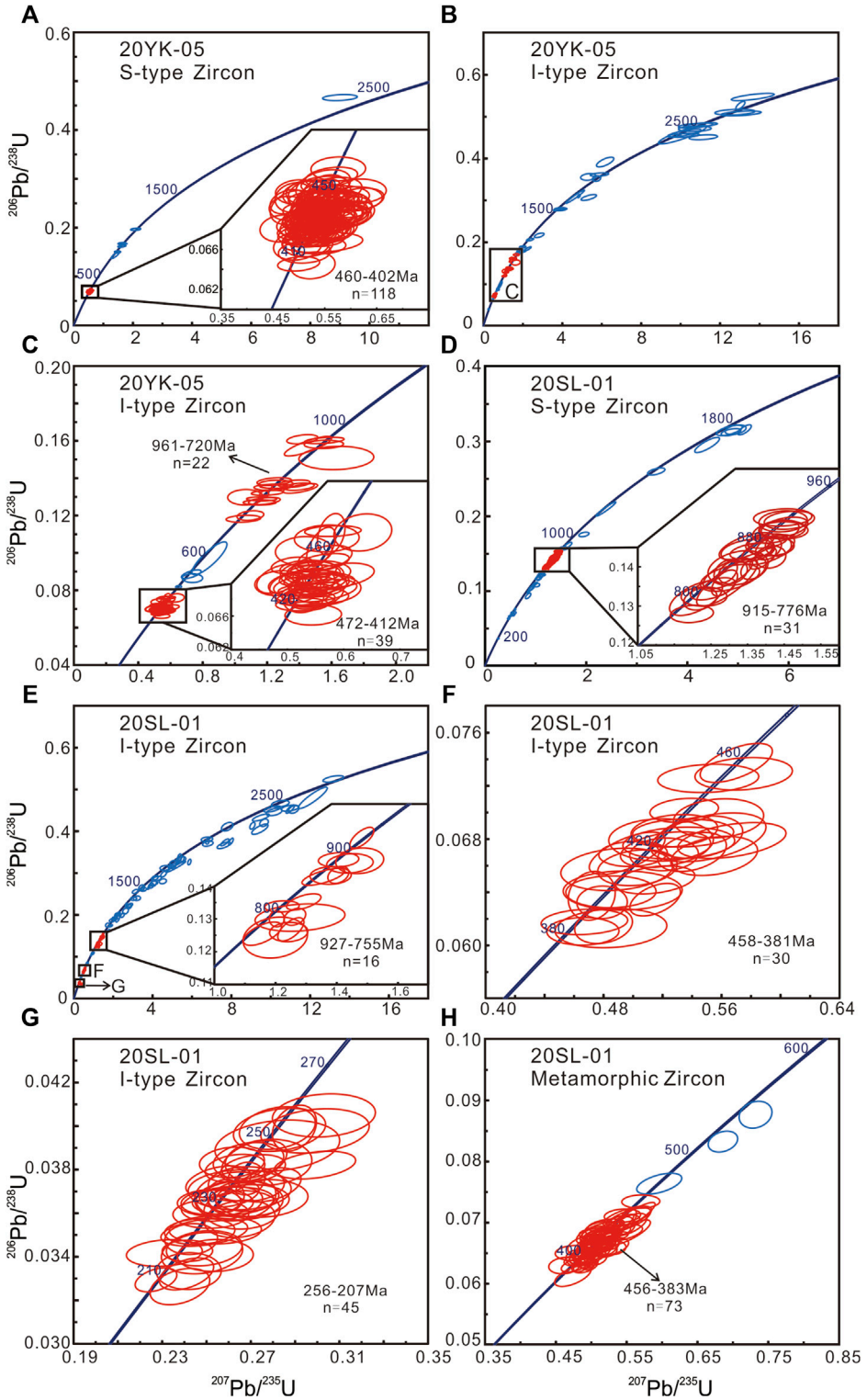


**FIGURE 6 |** U-Pb concordia plots for the main peaks of detrital zircon dates identified in **Figure 5**. **(A–C)** I- and S-Type zircon U-Pb concordia plots of Sample 20YK-05, **(D–G)** I- and S-Type zircon U-Pb concordia plots of Sample 20SL-01; **(H)** Metamorphic zircon U-Pb concordia plots of Sample 20SL-01.

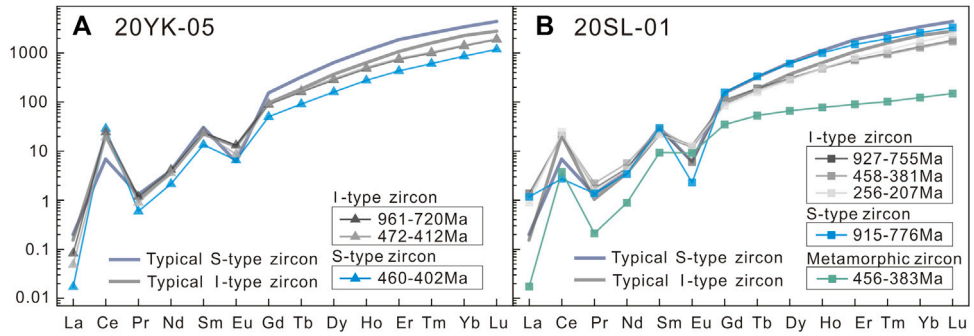


**FIGURE 7 |** REE in detrital zircons normalized to chondrite (normalization values from Sun and McDonough, 1989). **(A)** Sample 20YK-05, **(B)** Sample 20SL-01. The typical S and I-type zircon are collected from Burnham and Berry (2017) and Zhu et al. (2020).

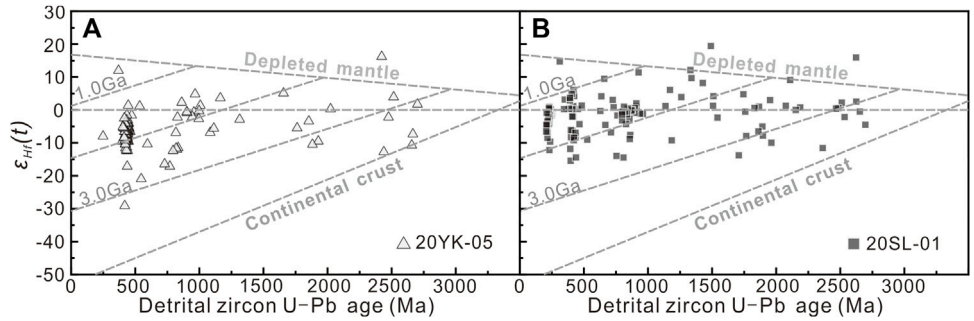


**FIGURE 8 | (A)** U-Pb age versus $\varepsilon_{Hf}$ (t) value plots of concordant detrital zircons of sample 20YK-05; **(B)** U-Pb age versus $\varepsilon_{Hf}$ (t) value plots of concordant detrital zircons of sample 20SL-01.

(**Figure 8A**), with only two grains with $\varepsilon_{Hf}$ (t) > 0, and $T_{DM2}$ in the range of 2.8–1.6 Ga (**Figures 9A-3**). Zircons in the range of 480–400 Ma yield values of $\varepsilon_{Hf}$ (t) in the range of −29.1–1.4 (**Figure 8A**), with only one grain with $\varepsilon_{Hf}$ (t) >0, and $T_{DM2}$ in the range of 3.3–1.3 Ga (**Figures 9A-4**).

Zircons from sample 20SL-01 (117 valid analyses) yield $\varepsilon_{Hf}$ (t) values in the range of −15.4–19.4 (**Figure 8B**), and $T_{DM2}$ ages in the range of 3.6–0.4 Ga (**Figures 9B-1**), with a peak in the range of 2.5–1.2 Ga. Zircon crystals with U–Pb ages of >1,000 Ma yield $\varepsilon_{Hf}$ (t) in the range of −13.8–15.9 (**Figure 8B**) and $T_{DM2}$ in the range of 3.6–1.4 Ga (**Figures 9B-2**). Zircons in the age range of 1,000–700 Ma yield $\varepsilon_{Hf}$ (t) in the range of −14.5–11.4 (**Figure 8B**) and $T_{DM2}$ varying from 2.6 to 1.1 Ga (**Figures 9B-3**). Zircons in the range of 460–380 Ma yield $\varepsilon_{Hf}$ (t) in the range of −14.5–6.1 (**Figure 8B**), with $T_{DM2}$ in the range of 2.4–1.0 Ga (**Figures 9B-4**). Zircons in the range of 260–200 Ma yield $\varepsilon_{Hf}$ (t) in the range of −12.2–0.9 (**Figure 8B**), with $T_{DM2}$ in the range of 2.1–1.2 Ga (**Figures 9B-5**).

# 5 DISCUSSION

## 5.1 Potential Source of the Detrital Zircons

Both samples were collected from the North Qaidam UHPM belt, but the upper reaches of the rivers extend beyond this belt. Therefore, analysis of the source(s) of the zircons should consider the contributions made by the upstream portions of the rivers. The Yuka River flows northeast to southwest, from the Qilian Terrane to the Qaidam Basin (**Figure 1E**). Its main tributaries are located in the Yuka area of Qaidam and the South Qilian Terrane. Therefore, investigation of provenance must consider the contribution of the South Qilian Terrane. While the Shaliu River flows southeast to northwest (**Figure 1F**), and its main tributaries are located in the eastern part of the East Kunlun orogenic belt and the North Qaidam UHPM belt. Provenance analysis therefore needs to combine the East Kunlun and North Qaidam.

Combining knowledge of the location of the ancient continents (Gehrels et al., 2003; Song et al., 2014; Wan et al., 2001; Wan et al., 2006), Nd isotopic data (Wan et al., 2006), and especially detrital zircon data (Tung et al., 2007; Xu et al., 2007; Liu et al., 2008; Sun et al., 2008; Sun et al., 2009; Wang et al., 2010; Wang et al., 2012; Wang et al., 2013; Chen et al., 2011; Gehrels et al., 2011; He et al., 2016; Yan et al., 2017; Meng et al., 2017; Jian et al., 2020), shows that the Precambrian basement detrital zircon U–Pb age peaks of the South Qilian, North Qaidam, and East Kunlun terranes are identical to those of the western Yangtze Block, indicating that these terranes have affinity to the western Yangtze Block (Gao and Zhang, 2017; Jian et al., 2020). In this

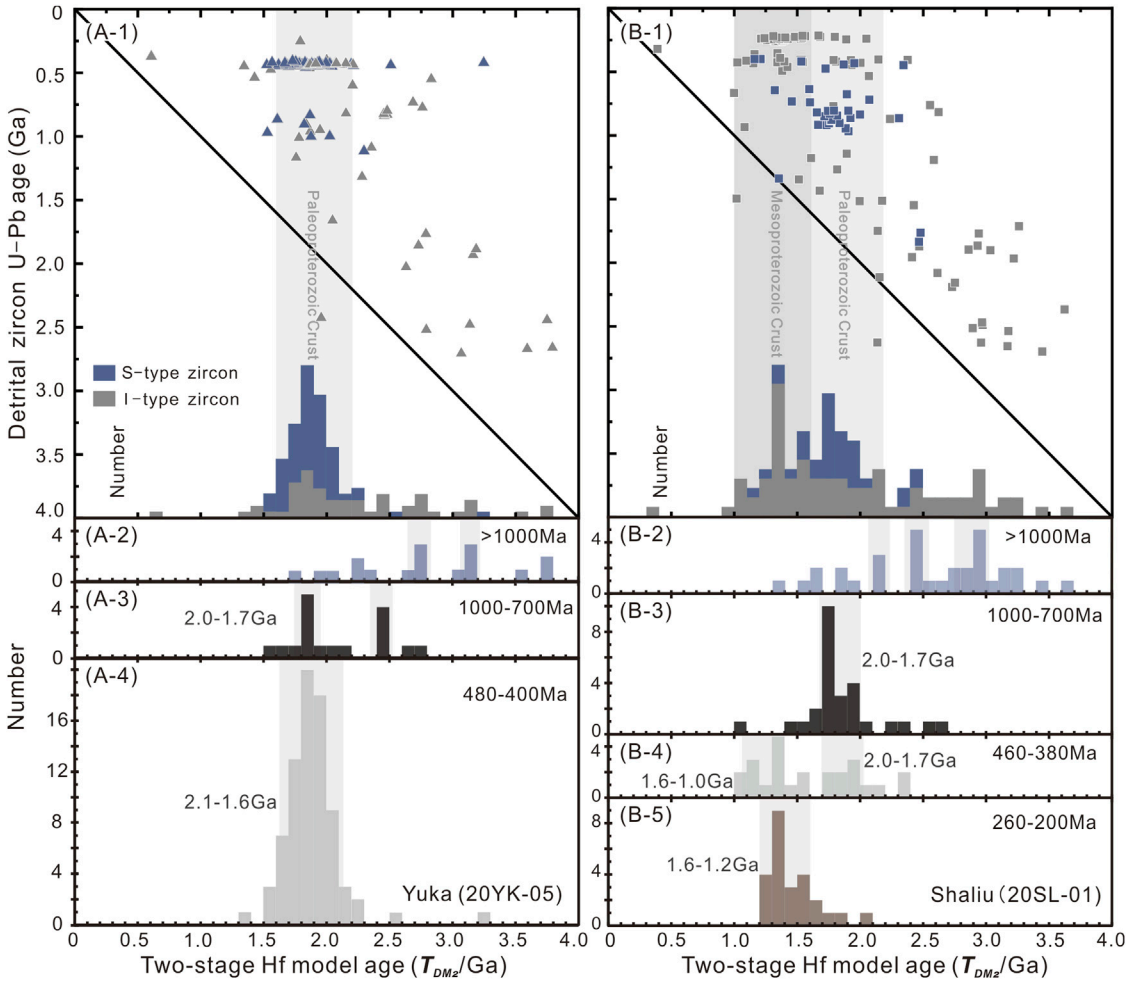


**FIGURE 9 |** U-Pb age versus two-stage Hf model age ($T_{DM2}$) value plots of concordant detrital zircons **(A-1)** Sample 20YK-05 **(B-1)** Sample 20SL-01; Relative probability plots of $T_{DM2}$ **(A-2,3,4)** Sample 20YK-05 **(B-2,3,4,5)** Sample 20SL-01.

study, 1,000–700 Ma detrital zircons from the North Qaidam and Qilian terrane (sample 20YK-05) related to the Rodinia supercontinent account for 12% of the sampled grains, and the corresponding 1,000–700 Ma detrital zircons from the North Qaidam and East Kunlun terrane (sample 20SL-01) account for 25%. The detrital zircons of two samples are both partly sourced from the North Qaidam terrane, so the difference in the proportion of Neoproterozoic zircon (13%) may be derived from two different terranes (the South Qilian and the East Kunlun terranes). The detrital zircon of the East Kunlun terrane in this range is significantly more than that in the South Qilian, which is the feature age of the western Yangtze Block (0.91–0.72 Ga, Liu et al., 2008). Therefore, we infer that in the Rodinia supercontinent, the East Kunlun, compared with the South Qilian, show more affinity to the western Yangtze Block.

To track the sources of each identified age range, detrital zircons from the Yuka River were classified into three groups of 961–720 Ma (I-type, n = 22), 472–412 Ma (I-type, n = 39) and 460–402 Ma (S-type, n = 118) based on their ages and compositions, whilst detrital zircons from the Shaliu River were grouped into five groups of 915–776 Ma (S-type, n = 31), 927–755 Ma (I-type, n = 16), 458–381 Ma (I-type, n = 30), 256–207 Ma (I-type, n = 45), and 456–383 Ma (metamorphic age, n = 73; **Figure 6**). Pre-Mesoproterozoic detrital zircons (>1000 Ma) from the Yuka and Shaliu rivers accounted for a small part of the total grains and derived from the ancient crystalline basement.

The South Qilian and North Qaidam terranes record break-up of the Rodinia supercontinent (900–800 Ma), Pan-African regional metamorphism (600–500 Ma), and subduction–collision metamorphism (ca. 450 Ma) (Liu et al., 2012). The zircon U–Pb geochronology of Yuka (Lin et al., 2006) and Xitieshan (Zhang et al., 2003) granitic gneisses in the North Qaidam suggests that a Neoproterozoic granite belt formed during the break-up of Rodinia, implying that Yuka detrital zircons with ages of 961–720 Ma (**Figure 6C**) may be related to the syn- or post-break-up period of the Rodinia supercontinent. Coincides with the ca. 430 Ma continental subduction involving the South Qilian

terrane (Song et al., 2009b), the age of subduction–collision metamorphism is consistent with the main age ranges of the Yuka detrital zircons (S-type, 460–402 and I-type, 472–412 Ma), with a peak of 433 Ma (**Figure 5A**). In addition, early Paleozoic magmatic activity in South Qilian–North Qaidam was characterized by myr and multiple episodes. He et al. (2020) divided the magmatism into five periods, namely, 470–450, 450–430, 430–410, 410–400, and 400–370 Ma; with 450–430 Ma as the peak period of granitoid intrusions, which is consistent with the Paleozoic age peak of the studied Yuka River detrital zircons (**Figure 5A**). Meanwhile, this Paleozoic age peak is also consistent with the peak metamorphic age of the Yuka eclogite (435–430 Ma, Song et al., 2009b), indicating that some of the detrital zircons in the Yuka River may have originated from syn-collision magmatic activity.

For the Shaliu River, the age distribution of zircons is more complex, suggesting that they have multiple sources. In the East Kunlun orogenic belt, Mesoproterozoic to Neoproterozoic magmatic intrusions are mainly S-type granites, which are considered to be related to the assembly and break-up of the Rodinia supercontinent (He et al., 2018; Yan et al., 2017). These compositional and temporal features are consistent with the dominance of S-type detrital zircons with Mesoproterozoic to Neoproterozoic ages identified in this study (**Figure 5B**). The geochronology of detrital zircons from gneissic granitoid in Hongshuihe, East Kunlun, indicates crystallization ages of 930–772 Ma (He et al., 2018), which are consistent with the age range of Neoproterozoic S-type zircons of the present study (915–776 Ma; **Figure 6D**). The Shaliu granitic gneiss gave the age of ~920 Ma (Lu, 2002; Chen et al., 2007), being consistent with the Shaliu S-type detrital zircons analyzed for our sample (**Figure 6D**). In summary, the Neoproterozoic detrital zircons analyzed in this study are possibly related to the assembly and break-up of the Rodinia supercontinent at 1,000–700 Ma (Lu, 1998).

Paleozoic intrusions in the East Kunlun orogenic belt are mainly granitic and dioritic, which show a peak crystallization age range of 440–390 Ma (He et al., 2018). UHP metamorphic rocks including eclogite and country paragneiss gave continental deep subduction time of 434–421 Ma for the North Qadaim (Song et al., 2006; 2009b), consistent with the early Devonian ages (433–418 Ma, **Figures 5C-2**) from the Shaliu River sample analyzed in this study. Furthermore, zircons with metamorphic rims constitute a greater proportion of Shaliu River sediments than that of Yuka River sediments, and the main age range of these metamorphic zircons is 456–383 Ma (Zhang et al., 2013, 2014, 2016), which coincides with the timing of oceanic subduction and continental collision and associated syn-metamorphic process in North Qaidam. Therefore, most of the studied detrital zircons in the age range of 458–381 Ma (**Figure 6F**) and with a peak of ca. 422 Ma may have originated from continental syn-collision magmatism, with a few originating from syn-metamorphic processes (**Figure 6H**) related to the above oceanic subduction and continental collision in North Qaidam. While no metamorphic zircons found in the Yuka river due to only a small fraction of its catchment located in the North Qaidam UHPM belt.

The geochronology of Indosinian granites from the East Kunlun orogenic belt can be divided into three stages: formation and expansion of ocean ridges (309–260 Ma); large-scale subduction of the oceanic plate (260–230 Ma); and intracontinental orogenesis (230–190 Ma) (Guo et al., 1998). Mesozoic intrusive rocks are widely distributed throughout the East Kunlun orogenic belt, including granite, granodiorite, and diorite (He et al., 2018), consistent with the 256–207 Ma detrital zircons from the Shaliu River (**Figure 6G**). Moreover, most of the 256–207 Ma zircons are I-type zircons (**Figure 5B**), and such compositions are generally associated with oceanic subduction, which suggests that the 256–207 Ma I-type zircons may have been derived from oceanic subduction and post-orogenic magmatism in East Kunlun during the Indosinian orogenic event.

## 5.2 Crustal Evolution of the South Qilian, North Qaidam, and East Kunlun Terranes

Zircon Hf isotopes can be used to trace the evolution of the crust. In most cases, a positive $\varepsilon_{Hf}$ (t) value indicates that the magma was sourced from depleted mantle; if the corresponding $T_{DM2}$ age was close to the crystallization age, the crust can be considered juvenile. In contrast, a negative $\varepsilon_{Hf}$ (t) indicates that the magma may have included recycled ancient continental crust, and the corresponding $T_{DM2}$ is much older than the crystallization age. For unmixed zircons not derived from a hybrid source with a negative $\varepsilon_{Hf}$ (t), the $T_{DM2}$ age can be used to estimate the formation time of ancient continental crust (Couzinié, et al., 2016; Geng et al., 2011; Hawkesworth and Kemp, 2006; Iizuka and Hirata, 2005; Kemp et al., 2006; Liu et al., 2008). Accordingly, Hf isotopes of the detrital zircons can help to understand the crustal growth and evolution of the South Qilian, North Qaidam, and East Kunlun terranes. The $\varepsilon_{Hf}$ (t) values exhibit a wide range from negative to positive for each of the major age ranges of the two samples (**Figures 8A,B**). This value distribution indicates the addition of recycled crustal materials in the magma from which the zircons crystallized; except for several Mesoproterozoic zircons, which show values identical to that of the depleted mantle, indicating the addition of juvenile crust (**Figures 8A,B**).

To facilitate the interpretation of crustal evolution processes in this study, detrital zircons from the Yuka River were classified into three groups with age ranges of >1,000, 1,000–700, and 480–400 Ma, and detrital zircons from the Shaliu River were classified into four groups with age ranges of >1,000, 1,000–700, 460–380, and 260–200 Ma. As shown in relative probability plot histograms of U–Pb ages of Yuka detrital zircons (**Figure 5A**), the >1,000 Ma detrital zircons account for only a small percentage. There is the low proportion of detrital zircon of 1.5–1.0 Ga (both U–Pb ages and two-stage Hf crustal model ages, **Figures 5A**, **9A–1**), suggesting that the South Qilian and North Qaidam terranes were tectonically relatively stable during the Mesoproterozoic. The $\varepsilon_{Hf}$ (t) values of most of the 1,000–700 and 480–400 Ma detrital zircons from the Yuka River are negative (**Figure 8A**), and the $T_{DM2}$ ages are mainly in almost the same ranges of 2.1–1.6 and 2.0–1.7 Ga (**Figures 9A-3, A-4**), respectively, indicating that crustal evolution in the South Qilian—North Qaidam was dominated by recycling of

Paleoproterozoic crust from the Neoproterozoic onward. The two most significant periods of crustal growth in North Qaidam and East Kunlun were 2.2–1.7 and 1.6–1.2 Ga, followed by 3.3–2.7 and 2.5–2.3 Ga (**Figure 9B-1**). Except for the $\varepsilon_{Hf}$ (t) values of Mesoproterozoic detrital zircons, which are mainly positive, the $\varepsilon_{Hf}$ (t) values of zircons with other ages are both positive and negative (**Figures 8A,B**), suggesting that the North Qaidam and East Kunlun terranes have been dominated by the remelting and rebuilding of ancient crust, except during the Mesoproterozoic, when the addition of juvenile crust dominated in the East Kunlun Terrane.

In contrast with sample 20YK-05 collected from Yuka river, Mesoproterozoic zircons from sample 20SL-01 are characterized by more depleted Hf isotopes (the $\varepsilon_{Hf}$ (t) values of zircons of the Shaliu sample at 1.6–1.0 Ga are mostly positive, **Figure 8B**). A comparison of the crustal evolution processes of the South Qilian–North Qaidam and East Kunlun terranes shows that there were differences in crustal growth during 1.6–1.0 Ga (**Figures 9A-1,B-1**). $T_{DM2}$ ages of early Paleozoic detrital zircons (480–400 Ma) from North Qaidam–East Kunlun (2.0–1.7 and 1.6–1.0 Ga, **Figures 9B-4**) are more diverse than those from South Qilian–North Qaidam (2.1–1.6 Ga, **Figures 9A-4**), with a record of Mesoproterozoic continental crust (1.6–1.0 Ga). Moreover, the $T_{DM2}$ ages of 260–200 Ma detrital zircons from the North Qaidam and East Kunlun terranes are Mesoproterozoic (1.6–1.0 Ga, **Figures 9B-5**), also indicating a difference in crustal growth between South Qilian–North Qaidam and North Qaidam–East Kunlun, both of which were located adjacent to the western margin of the Yangtze Block, since at least 1.6 Ga. This difference may be related to the break-up of the Columbian supercontinent during 1.6–1.2 Ga (Hou et al., 2009; Wu et al., 2012; Yin et al., 2012; Wang et al., 2014, 2015; Deng et al., 2020).

## 5.3 Tectonic Evolution of the Northern Tibetan Plateau

### 5.3.1 Neoproterozoic Evolution

Jian et al. (2020) has studied detrital zircon U–Pb ages and Hf isotopes of Proterozoic and Paleozoic metamorphic sedimentary rocks from East Kunlun and showed that 1.0–0.9 Ga intrusions in the three terranes of South Qilian, North Qaidam, and East Kunlun are consistent with the age distribution of detrital zircons from East Kunlun and may record the Greenville orogeny. Therefore, these terranes may have been located on the same landmass during the Neoproterozoic. In addition to the above-mentioned evidence for the sources of detrital zircons, U–Pb ages of detrital zircons from Precambrian basement in the South Qilian, North Qaidam, and East Kunlun terranes have similar age clusters in the range of 1,000–700 Ma, which is consistent with the main age interval of 910–720 Ma of magmatic rocks in the western margin of the Yangtze Block (Liu et al., 2008). Moreover, $T_{DM2}$ ages of 1,000–700 Ma detrital zircons of the South Qilian and the East Kunlun terranes are clustered mainly between 2.0 and 1.5 Ga, with a peak of 1.8–1.7 Ga (**Figures 9A-3,B-3**), which also implies that the South Qilian, North Qaidam, and East Kunlun terranes may have been located within the same ancient continent at 1,000–700 Ma, most likely as part of the Rodinia supercontinent.

### 5.3.2 Early Paleozoic Evolution

Given that the main magmatic period (480–400 Ma) of the South Qilian Terrane preceded than that of the East Kunlun Terrane (460–380 Ma) and that the $T_{DM2}$ ages of early Paleozoic detrital zircons from the East Kunlun Terrane suggest the involvement of Mesoproterozoic continental crust (1.6–1.0 Ga), the East Kunlun and South Qilian terranes may not have been part of the same continent during the early Paleozoic. As such, we propose an archipelago model (Zhang et al., 2020), whereby the terranes were separated from each other by ocean basins during 525–480 Ma. The subduction of the South Qilian Ocean has started by ca. 480 Ma, and the ocean has closed by ca. 420 Ma. Subduction in the Proto-Tethys Ocean in South Qaidam had started by ca. 460 Ma, and the ocean had closed completely by ca. 400 Ma.

Zircon U–Pb ages of I-type granite related to oceanic subduction in the South Qilian–North Qaidam orogenic belt are in the range of 470–460 Ma (Wu et al., 2007), which is consistent with the age peak of I-type detrital zircons in the present study (472 Ma; **Figures 5C-1**) and with 473–443 Ma Shaliuhe oceanic eclogite representing the subduction of oceanic crust (Song et al., 2009b; Zhang et al., 2013). Therefore, subduction-related magmatism occurred at ca. 470 Ma in the North Qaidam UHPM belt. As the temperature increased, the subducted slabs were dehydrated and melted to form magmas, which assimilated continental crust during ascent to form I-type granitic magmas (negative $\varepsilon_{Hf}$ (t) values; **Figure 8A**) at ca. 470 Ma (**Figures 5C-1**). As the Proto-Tethys ocean closed, the subducting oceanic plate dragged the continental crust downward to also be subducted, and the Qilian Terrane was thrust southward over the Qaidam Terrane. The increase in the thickness of the continental crust caused by continental collision, coupled with the fluid formed by slab dehydration, caused partial melting of the continental crust, forming syn-orogenic S-type granitic magma at ca. 442 Ma (**Figures 5C-1**).

In most cases, the collision margin of the South Qilian–North Qaidam orogenic belt was irregular, and the pole of convergence of the collision was oblique rather than normal (Xu et al., 2013). Therefore, these oblique and irregular edges would have caused asynchronous timings of collision in different parts of the collision zone, which may have led to multiple episodes of magmatism in the orogenic belt. This is reflected in the multiple age peaks of detrital zircons (**Figures 5C,D**). From 437 to 424 Ma, I-type granitic magmatism related to oceanic subduction occurred in the Yuka area (**Figures 5C-1**). In addition to the 442 Ma S-type granitic magmatism, 433 Ma S-type granitic magmatism is also recorded in the South Qilian and North Qaidam terranes (**Figures 5C-1**). Asynchronous collision caused the I-type granitic magmatism related to oceanic subduction in the North Qaidam and East Kunlun terranes (started at 453 Ma) to occur 17 Myr later than that in the South Qilian Terrane, and the major I-type peak of Shaliu sample (ca. 418 Ma, **Figure 5C**) are decoupled with the major I-type peak of Yuka sample (ca. 437 Ma). The oceanic subduction

was still occurring in some localities at 418 Ma (**Figures 5C-2**). However, a few S-type granites in the North Qaidam and East Kunlun terranes were formed at 433 Ma (**Figures 5C-2**), which is consistent with the 433 Ma S-type granites in the Yuka area, indicating that large-scale granites were produced in North Qaidam during continental collision.

Zhou et al. (2021) showed that mafic dikes with ages of 393–375 Ma were derived from the melting of the lithosphere mantle in Dulan, North Qaidam. These dikes were derived from the melting of the mantle peridotite, which mark the initiation of post-collisional magmatism in an orogen. The timing of the formation of these mafic dikes coincides with I-type magmatism (ca. 397 and ca. 385 Ma; **Figures 5C-2**) during the middle Devonian in the North Qaidam and East Kunlun terranes. Therefore, we speculate that the I-type granite of the middle Devonian (ca. 397–385 Ma) was the product of the partial melting of the lithospheric mantle which assimilated the continental crust during the late magmatic evolution.

### 5.3.3 Late Paleozoic–Early Mesozoic Evolution

Late Paleozoic to early Mesozoic granitic intrusions are widely distributed in the eastern part of the East Kunlun Terrane, and their formation might be related with the Paleo-Tethyan oceanic subduction (Li et al., 2012a, b; Ma et al., 2015). This subduction occurred during the late Permian to Middle Triassic and eventually led to closure of the Paleo-Tethys Ocean (Buqingshan Ocean) in southern East Kunlun. In this study, 260–200 Ma I-type magmatic zircons, with peak ages of ca. 252 Ma, ca. 241 Ma, ca. 231 Ma, ca. 222 Ma, and ca. 217 Ma, could be formed by multi-stage magmatism associated with this oceanic subduction process. According to the zircon probability density plots (**Figure 5D**), northward Paleo-Tethys oceanic plate subduction (Cheng et al., 2017; Gehrels et al., 2011; Jian et al., 2020; Xiong et al., 2014; Zhang et al., 2020) started during the late Permian (ca. 260–252 Ma) and continued intensely through to the middle Triassic (ca. 231 Ma), and in a more subdued manner until the Late Triassic (ca. 217–200 Ma).

In summary, the South Qilian, North Qaidam, and East Kunlun terranes have undergone multiple Wilson cycles since the Paleoproterozoic. These terranes/microcontinents were located on the same major ancient continent during 2.1–1.6 Ga and subsequently separated during 1.6–1.2 Ga. The East Kunlun Terrane was augmented by the juvenile crust at this stage, whereas the Qilian Terrane was relatively stable in tectonic and magmatic terms. By ca. 1,000 Ma, as a result of the assembly of the Rodinia supercontinent, the three microcontinents (South Qilian, North Qaidam, and East Kunlun) reassembled on the western Yangtze block, while the East Kunlun terrane was closer than other two terranes, and then became separated by the Proto-Tethys Ocean during the break-up of Rodinia. Later, the Proto-Tethys Ocean began to close, and the three continents collided with each other after closure of the Paleo-Tethys Ocean, forming the current configuration and structure of the South Qilian, North Qaidam, and East Kunlun terranes.

## 6 CONCLUSION

To investigate the evolution of continental crust of the northern Tibetan Plateau, detrital zircon U–Pb geochronology and Hf isotope analysis by LA-(MC)-ICPMS was performed on two fluvial sand samples from North Qaidam (the Yuka and Shaliu rivers). The main conclusions of the study are as follows.

1) Age distributions of detrital zircons from the Yuka River cluster mainly in two ranges of 1,000–700 and 480–400 Ma, with age peaks at 820 and 433 Ma, respectively. Corresponding data for Shaliu River falls in the ranges of 1,000–700, 460–380, and 260–200 Ma, with peaks of 875, 422, and 232 Ma, respectively.
2) Detrital zircon U–Pb geochronology and Hf isotope analysis show that the Qilian, North Qaidam, and East Kunlun terranes show affinity to the western Yangtze Block.
3) The presence of Mesoproterozoic continental crust (1.6–1.0 Ga) in the East Kunlun and North Qaidam terranes indicate differences in crustal evolution between the East Kunlun–Qaidam terranes and the Qilian Terrane. Phanerozoic magmatic records for the South Qilian, North Qaidam, and East Kunlun terranes suggest that the magmas were mainly sourced from recycled ancient continental crust with minor contributions from the juvenile crust.
4) The Qilian, North Qaidam, and East Kunlun terranes have undergone multiple Wilson cycles since the Paleoproterozoic. We suggest an archipelago model for part of their evolution, which proposes that the terranes were separated from each other by ocean basins during 525–480 Ma.

## DATA AVAILABILITY STATEMENT

The original contributions presented in the study are included in the article/**Supplementary Material**, further inquiries can be directed to the corresponding author.

## AUTHOR CONTRIBUTIONS

GZ designed this project, GZ, LX, FC and SL collected all samples of this study and field investigation, ZL conducted most of laboratory analysis and data explanation, GZ and ZL wrote the manuscript.

## FUNDING

This study is supported by the National Natural Science Foundation of China (Grants 91755206, 41972056, and 41622202).

## SUPPLEMENTARY MATERIAL

The Supplementary Material for this article can be found online at: https://www.frontiersin.org/articles/10.3389/feart.2022.866375/full#supplementary-material

## REFERENCES


Belousova, E. A., Kostitsyn, Y. A., Griffin, W. L., Begg, G. C., O'Reilly, S. Y., and Pearson, N. J. (2010). The Growth of the Continental Crust: Constraints from Zircon Hf-Isotope Data. *Lithos* 119, 457–466. doi:10.1016/j.lithos.2010.07.024

Belousova, E., Griffin, W., O'Reilly, S. Y., and Fisher, N. (2002). Igneous Zircon: Trace Element Composition as an Indicator of Source Rock Type. *Contrib. Mineral. Petrol.* 143, 602–622. doi:10.1007/s00410-002-0364-7

Blayney, T., Najman, Y., Dupont-Nivet, G., Carter, A., Millar, I., Garzanti, E., et al. (2016). Indentation of the Pamirs with Respect to the Northern Margin of Tibet: Constraints from the Tarim Basin Sedimentary Record. *Tectonics* 35, 2345–2369. doi:10.1002/2016TC004222

Blichert-Toft, J., Chauvel, C., and Albarède, F. (1997). Separation of Hf and Lu for High-Precision Isotope Analysis of Rock Samples by Magnetic Sector-Multiple Collector ICP-MS. *Contrib. Mineralogy Petrology* 127, 248–260. doi:10.1007/s004100050278

Botsyun, S., Sepulchre, P., Donnadieu, Y., Risi, C., Licht, A., and Caves Rugenstein, J. K. (2019). Revised Paleoaltimetry Data show low Tibetan Plateau Elevation during the Eocene. *Science* 363, eaaq1436. doi:10.1126/science.aaq1436

Burnham, A. D., and Berry, A. J. (2017). Formation of Hadean Granites by Melting of Igneous Crust. *Nat. Geosci* 10, 457–461. doi:10.1038/ngeo2942

Chen, J.-F., Han, B.-F., Zhang, L., Xu, Z., Liu, J.-L., Qu, W.-J., et al. (2015). Middle Paleozoic Initial Amalgamation and Crustal Growth in the West Junggar (NW China): Constraints from Geochronology, Geochemistry and Sr-Nd-Hf-Os Isotopes of Calc-Alkaline and Alkaline Intrusions in the Xiemisitai-Saier Mountains. *J. Asian Earth Sci.* 113, 90–109. doi:10.1016/j.jseaes.2014.11.028

Chen, N., Xia, X., Li, X., Sun, M., Xu, P., Liu, X., et al. (2007). Timing of Magmatism of the Gneissic-Granite Plutons along North Qaidam Margin and Implications for Precambrian Crustal Accretions: Zircon U-Pb Dating and Hf Isotope Evidences. *Acta Petrol. Sin.* 23, 501–512. in Chinese with English abstract.

Chen, Y., Pei, X., Li, R., Liu, Z., Li, Z., Zhang, X., et al. (2011). Zircon U-Pb Age of Xiaomiao Formation of Proterozoic in the Eastern Section of the East Kunlun Orogenic Belt. *Geoscience* 25, 510–521. in Chinese with English abstract.

Cheng, F., Jolivet, M., Hallot, E., Zhang, D., Zhang, C., and Guo, Z. (2017). Tectono-Magmatic Rejuvenation of the Qaidam Craton, Northern Tibet. *Gondwana Res.* 49, 248–263. doi:10.1016/j.gr.2017.06.004

Clark, M. K., Farley, K. A., Zheng, D., Wang, Z., and Duvall, A. R. (2010). Early Cenozoic Faulting of the Northern Tibetan Plateau Margin from Apatite (U-Th)/He Ages. *Earth Planet. Sci. Lett.* 296, 78–88. doi:10.1016/j.epsl.2010.04.051

Condie, K. C., Beyer, E., Belousova, E., Griffin, W. L., and O'Reilly, S. Y. (2005). U-pb Isotopic Ages and Hf Isotopic Composition of Single Zircons: The Search for Juvenile Precambrian continental Crust. *Precambrian Res.* 139, 42–100. doi:10.1016/j.precamres.2005.04.006

Corfu, F., Hanchar, J. M., Hoskin, P. W. O., and Kinny, P. (2003). 16. Atlas of Zircon Textures. *Rev. Mineral. Geochem.* 53, 469–502. doi:10.2113/0530469

Couzinié, S., Laurent, O., Moyen, J.-F., Zeh, A., Bouilhol, P., and Villaros, A. (2016). Post-collisional Magmatism: Crustal Growth Not Identified by Zircon Hf-O Isotopes. *Earth Planet. Sci. Lett.* 456, 182–195. doi:10.1016/j.epsl.2016.09.033

Deng, Q., Wang, Z., Ren, G., Cui, X., Cao, H., Ning, K., et al. (2020). Identification of the –2.09 Ga and –1.76 Ga Granitoids in the Northwestern Yangtze Block: Records of the Assembly and Break-Up of Columbia Supercontinent. *Earth Sci.* 45, 3295–3312. in Chinese with English abstract. doi:10.3799/dqkx.2020.182

Gao, Z., and Zhang, G. (2017). Geochronology of Detrital Zircons from Metapelite of the North Qaidam UHPM Belt and its Geological Implications. *Acta Petrol. Sin.* 33, 1775–1788. in Chinese with English abstract.

Gehrels, G. E., Yin, A., and Wang, X.-F. (2003). Detrital-zircon Geochronology of the Northeastern Tibetan Plateau. *Geol. Soc. Am. Bull.* 115, 881–896. doi:10.1130/0016-7606(2003)115<0881:dgotnt>2.0.co;2

Gehrels, G., Kapp, P., DeCelles, P., Pullen, A., Blakey, R., Weislogel, A., et al. (2011). Detrital Zircon Geochronology of Pre-tertiary Strata in the Tibetan-Himalayan Orogen. *Tectonics* 30, a–n. doi:10.1029/2011TC002868

Geng, X., Gao, S., and Chen, C. (2011). Crustal Growth of the Eastern North China Craton and Sulu Orogen as Revealed by U-Pb Dating and Hf Isotopes of Detrital Zircons from Modern Rivers. *Earth Sci.* 36, 483–499. in Chinese with English abstract. doi:10.3799/dqkx.2011.050

Gong, H., Zhao, H., Xie, W., Kang, W., Zhang, R., Yang, L., et al. (2017). Tectono-Thermal Events of the North Qilian Orogenic Belt, NW China: Constraints from Detrital Zircon U-Pb Ages of Heihe River Sediments. *J. Asian Earth Sci.* 138, 647–656. doi:10.1016/j.jseaes.2017.03.003

Griffin, W. L., Pearson, N. J., Belousova, E., Jackson, S. E., van Achterbergh, E., O'Reilly, S. Y., et al. (2000). The Hf Isotope Composition of Cratonic Mantle: LAM-MC-ICPMS Analysis of Zircon Megacrysts in Kimberlites. *Geochimica et Cosmochimica Acta* 64, 133–147. doi:10.1016/S0016-7037(99)00343-9

Guo, Z., Deng, J., Xu, Z., Mo, X., and Luo, Z. (1998). Late Paleozoic-Mesozoic Intracontinental Orogenic Process and Intermediate-Acidic Igneous Rocks from the Eastern Kunlun Mountains of North Western China. *Geoscience* 12, 344–352. in Chinese with English abstract.

Hawkesworth, C. J., and Kemp, A. I. S. (2006). Evolution of the Continental Crust. *Nature* 443, 811–817. doi:10.1038/nature05191

He, D., Dong, Y., Liu, X., Yang, Z., Sun, S., Cheng, B., et al. (2016). Tectono-thermal Events in East Kunlun, Northern Tibetan Plateau: Evidence from Zircon U-Pb Geochronology. *Gondwana Res.* 30, 179–190. doi:10.1016/j.gr.2015.08.002

He, D., Dong, Y., Liu, X., Zhou, X., Zhang, F., and Sun, S. (2018). Zircon U-Pb Geochronology and Hf Isotope of Granitoids in East Kunlun: Implications for the Neoproterozoic Magmatism of Qaidam Block, Northern Tibetan Plateau. *Precambrian Res.* 314, 377–393. doi:10.1016/j.precamres.2018.06.017

He, X., Yang, X., Wang, Y., Guo, R., Liao, Y., and Fan, Y. (2020). Petrology, Geochemistry and Zircon U-Pb Geochronology of the Chaidamushan Granite from the Southern Margin of Qilianshan. *Acta Geol. Sin.* 94, 1248–1263. in Chinese with English abstract10.1111/1755-6724.14347.

Hoskin, P. W. O., and Black, L. P. (2000). Metamorphic Zircon Formation by Solid-State Recrystallization of Protolith Igneous Zircon. *J. Metamorphic Geology.* 18, 423–439. doi:10.1046/j.1525-1314.2000.00266.x

Hou, G., Halls, H., Davis, D., Huang, B., Yang, M., and Wang, C. (2009). Paleomagnetic Poles of Mafic Dyke Swarms from the North China Craton and Their Relevance to the Reconstruction of the Supercontinent Columbia. *Acta Petrol. Sin.* 25, 650–658. in Chinese with English abstract.

Iizuka, T., and Hirata, T. (2005). Improvements of Precision and Accuracy in *In Situ* Hf Isotope Microanalysis of Zircon Using the Laser Ablation-MC-ICPMS Technique. *Chem. Geology.* 220, 121–137. doi:10.1016/j.chemgeo.2005.03.010

Jackson, S. E., Pearson, N. J., Griffin, W. L., and Belousova, E. A. (2004). The Application of Laser Ablation-Inductively Coupled Plasma-Mass Spectrometry to *In Situ* U-Pb Zircon Geochronology. *Chem. Geology.* 211, 47–69. doi:10.1016/j.chemgeo.2004.06.017

Jian, X., Weislogel, A., Pullen, A., and Shang, F. (2020). Formation and Evolution of the Eastern Kunlun Range, Northern Tibet: Evidence from Detrital Zircon U-Pb Geochronology and Hf Isotopes. *Gondwana Res.* 83, 63–79. doi:10.1016/j.gr.2020.01.015

Kang, H., Chen, Y., Li, D., Bao, C., Chen, Y., Xue, H., et al. (2019). Detrital Zircon Record of Rivers' Sediments in the North Qilian Orogenic Belt: Implications of the Tectonic Evolution of the Northeastern Tibetan Plateau. *Geol. J.* 54, 2208–2228. doi:10.1002/gj.3291

Kemp, A. I. S., Hawkesworth, C. J., Paterson, B. A., and Kinny, P. D. (2006). Episodic Growth of the Gondwana Supercontinent from Hafnium and Oxygen Isotopes in Zircon. *Nature* 439, 580–583. doi:10.1038/nature04505

Kröner, A., Kovach, V., Belousova, E., Hegner, E., Armstrong, R., Dolgopolova, A., et al. (2014). Reassessment of Continental Growth during the Accretionary History of the Central Asian Orogenic Belt. *Gondwana Res.* 25, 103–125. doi:10.1016/j.gr.2012.12.023

Kui, M., Bai, H., Gu, F., and Miao, G. (2010). Division of East Kunlun Tectonic Magmatic Belt and the Rock Tectonic Combination in the Late Variscan-Yanshanian Period. *J. Qinghai Univ. (Nature Science)* 28, 49–55. in Chinese with English abstract.

Lease, R. O., Burbank, D. W., Gehrels, G. E., Wang, Z., and Yuan, D. (2007). Signatures of Mountain Building: Detrital Zircon U/Pb Ages from Northeastern Tibet. *Geol* 35, 239–242. doi:10.1130/g23057a.1

Li, B., Sun, F., Yu, X., Qian, Y., Wang, G., and Yang, Y. (2012a). U-pb Dating and Geochemistry of Diorite in the Eastern Section from Eastern Kunlun Middle Uplifted Basement and Granitic Belt. *Acta Petrol. Sin.* 28, 1163–1172. in Chinese with English abstract.

Li, H., Lu, S., Zhao, F., Li, H., and Yu, H. (1999). Geochronological Framework of the Neoproterozoic Major Geological Events in the Northern Margin of the Qaidam Basin. *Geoscience* 2, 224–225. in Chinese with English abstract.

Li, R., Pei, X., Li, Z., Liu, Z., Chen, G., Chen, Y., et al. (2012b). Geological Characteristics of Late Palaeozoic-Mesozoic Unconformities and Their Response to Some Significant Tectonic Events in Eastern Part of Eastern Kunlun. *Earth Sci. Front.* 19, 244–254. in Chinese with English abstract.

Li, X.-H., Long, W.-G., Li, Q.-L., Liu, Y., Zheng, Y.-F., Yang, Y.-H., et al. (2010). Penglai Zircon Megacrysts: A Potential New Working Reference Material for Microbeam Determination of Hf-O Isotopes and U-Pb Age. *Geostand. Geoanal. Res.* 34, 117–134. doi:10.1111/j.1751-908X.2010.00036.x

Lin, C., Sun, Y., Chen, D., and Diwu, C. (2006). Geochemistry and Zircon LA-ICPMS Dating of Iqe River Granitic Gneiss, Northern Margin of Qaidam Basin. *Geochimica* 5, 489–505. in Chinese with English abstract.

Liu, X., Gao, S., Diwu, C., and Ling, W. (2008). Precambrian Crustal Growth of Yangtze Craton as Revealed by Detrital Zircon Studies. *Am. J. Sci.* 308, 421–468. doi:10.2475/04.2008.02

Liu, Y., Neubauer, F., Li, W., Genser, J., and Li, W. (2012). Tectono-Thermal Events of the Northern Qaidam Margin-Southern Qilian Area, Western China. *J. Jilin Univ. (Earth Sci. Edition)* 42, 1317–1329. in Chinese with English abstract.

Lu, S. N. (1998). A Review of Advance in the Research on the Neoproterozoic Rodinia Supercontinent. *Geol. Rev.* 44, 489–495. in Chinese with English abstract.

Lu, S. N. (2002). *Preliminary Study on Precambrian Geology of Northern Qinghai-Tibet Plateau*. Beijing: Geological Publishing House.

Lu, X., Sun, Y., Zhang, X., Xiao, Q., Wang, X., and Wei, X. (2007). The SHRIMP Age of Tatalin Rapakivi Granite at the North Margin of Qaidam Basin. *Acta Geol. Sin.* 81, 626–634. in Chinese with English abstract.

Ludwig, K. R. (2003). *Isoplot 3.00: A Geochronological Toolkit for Microsoft Excel*. Berkeley CA: Berkeley Geochronology Center. 4, 0-71.

Ma, C., Xiong, F., Yin, S., Wang, L., and Gao, K. (2015). Intensity and Cyclicity of Orogenic Magmatism: An Example from a Paleo-Tethyan Granitoid Batholith, Eastern Kunlun, Northern Qinghai-Tibetan Plateau. *Acta Petrol. Sin.* 31, 3555–3568. in Chinese with English abstract.

Meng, F., Jia, L., Ren, Y., Liu, Q., and Duan, X. (2017). Magmatic and Metamorphic Events Recorded in the Gneisses of the Wenquan Region, East Kunlun Mountains, Northwest China: Evidence from the Zircon U-Pb Geochronology. *Acta Petrol. Sin.* 33, 3691–3709. in Chinese with English abstract.

Nie, J., Horton, B. K., Saylor, J. E., Mora, A., Mange, M., Garzione, C. N., et al. (2012). Integrated Provenance Analysis of a Convergent Retroarc Foreland System: U-Pb Ages, Heavy Minerals, Nd Isotopes, and sandstone Compositions of the Middle Magdalena Valley basin, Northern Andes, Colombia. *Earth-Science Rev.* 110, 111–126. doi:10.1016/j.earscirev.2011.11.002

Patchett, P. J., and Tatsumoto, M. (1981). A Routine High-Precision Method for Lu-Hf Isotope Geochemistry and Chronology. *Contr. Mineral. Petrol.* 75, 263–267. doi:10.1007/BF01166766

Paton, C., Hellstrom, J., Paul, B., Woodhead, J., and Hergt, J. (2011). Iolite: Freeware for the Visualisation and Processing of Mass Spectrometric Data. *J. Anal. Spectrom.* 26, 2508–2518. doi:10.1039/c1ja10172b

Pearce, N. J. G., Perkins, W. T., Westgate, J. A., Gorton, M. P., Jackson, S. E., Neal, C. R., et al. (1997). A Compilation of New and Published Major and Trace Element Data for NIST SRM 610 and NIST SRM 612 Glass Reference Materials. *Geostand. Newsl.* 21, 115–144. doi:10.1111/j.1751-908X.1997.tb00538.x

Rohrmann, A., Kapp, P., Carrapa, B., Reiners, P. W., Guynn, J., Ding, L., et al. (2012). Thermochronologic Evidence for Plateau Formation in central Tibet by 45 Ma. *Geology* 40, 187–190. doi:10.1130/G3253010.1130/g32530.1

Rubatto, D. (2002). Zircon Trace Element Geochemistry: Partitioning with Garnet and the Link between U-Pb Ages and Metamorphism. *Chem. Geology.* 184, 123–138. doi:10.1016/S0009-2541(01)00355-2

Sláma, J., Košler, J., Condon, D. J., Crowley, J. L., Gerdes, A., Hanchar, J. M., et al. (2008). Plešovice Zircon - A New Natural Reference Material for U-Pb and Hf Isotopic Microanalysis. *Chem. Geology.* 249, 1–35. doi:10.1016/j.chemgeo.2007.11.005

Song, B., Zhang, K., Hou, Y., Ji, J., Wang, J., Yang, Y., et al. (2019a). New Insights into the Provenance of Cenozoic Strata in the Qaidam Basin, Northern Tibet: Constraints from Combined U-Pb Dating of Detrital Zircons in Recent and Ancient Fluvial Sediments. *Palaeogeogr. Palaeoclimatol. Palaeoecol.* 533, 109254. doi:10.1016/j.palaeo.2019.109254

Song, S., Bi, H., Qi, S., Yang, L., Allen, M. B., Niu, Y., et al. (2018). HP-UHP Metamorphic Belt in the East Kunlun Orogen: Final Closure of the Proto-Tethys Ocean and Formation of the Pan-North-China Continent. *J. Petrol.* 59, 2043–2060. doi:10.1093/petrology/egy089

Song, S. G., Yang, J. S., Xu, Z. Q., Liou, J. G., and Shi, R. D. (2003). Metamorphic Evolution of the Coesite-Bearing Ultrahigh-Pressure Terrane in the North Qaidam, Northern Tibet, NW China. *J. Metamorph. Geol.* 21, 631–644. doi:10.1046/j.1525-1314.2003.00469.x

Song, S., Niu, Y., Su, L., and Xia, X. (2013). Tectonics of the North Qilian Orogen, NW China. *Gondwana Res.* 23, 1378–1401. doi:10.1016/j.gr.2012.02.004

Song, S., Niu, Y., Su, L., Zhang, C., and Zhang, L. (2014). Continental Orogenesis from Ocean Subduction, Continent Collision/Subduction, to Orogen Collapse, and Orogen Recycling: The Example of the North Qaidam UHPM belt, NW China. *Earth-Science Rev.* 129, 59–84. doi:10.1016/j.earscirev.2013.11.010

Song, S., Niu, Y., Zhang, L., and Zhang, G. (2009b). Time Constraints on Orogenesis from Oceanic Subduction to Continental Subduction, Collision, and Exhumation: An Example from North Qilian and North Qaidam HP-UHP Belts. *Acta Petrol. Sin.* 25, 2067–2077. in Chinese with English abstract.

Song, S., Su, L., Niu, Y., Zhang, G., and Zhang, L. (2009a). Two Types of Peridotite in North Qaidam UHPM belt and Their Tectonic Implications for Oceanic and Continental Subduction: A Review. *J. Asian Earth Sci.* 35, 285–297. doi:10.1016/j.jseaes.2008.11.009

Song, S., Wu, Z., Yang, L., Su, L., Xia, X., Wang, C., et al. (2019b). Ophiolite Belts and Evolution of the Proto-Tethys Ocean in the Qilian Orogen. *Acta Petrol. Sin.* 35, 2948–2970. in Chinese with English abstract.

Song, S., Zhang, C., Li, X., and Zhang, L. (2011). HP/UHP Metamorphic Time of Eclogite in the Xitieshan Terrane, North Qaidam UHPM belt, NW China. *Acta Petrol. Sin.* 27, 1191–1197. in Chinese with English abstract.

Song, S., Zhang, L., Niu, Y., Su, L., Song, B., and Liu, D. (2006). Evolution from Oceanic Subduction to Continental Collision: a Case Study from the Northern Tibetan Plateau Based on Geochemical and Geochronological Data. *J. Petrol.* 47, 435–455. doi:10.1093/petrology/egi080

Sun, J.-F., Yang, J.-H., Wu, F.-Y., and Wilde, S. A. (2012). Precambrian Crustal Evolution of the Eastern North China Craton as Revealed by U-Pb Ages and Hf Isotopes of Detrital Zircons from the Proterozoic Jing'eryu Formation. *Precambrian Res.* 200-203, 184–208. doi:10.1016/j.precamres.2012.01.018

Sun, S.-s., and McDonough, W. F. (1989). Chemical and Isotopic Systematics of Oceanic Basalts: Implications for Mantle Composition and Processes. *Geol. Soc. Lond. Spec. Publications* 42, 313–345. doi:10.1144/gsl.sp.1989.042.01.19

Sun, W.-H., Zhou, M.-F., Gao, J.-F., Yang, Y.-H., Zhao, X.-F., and Zhao, J.-H. (2009). Detrital Zircon U-Pb Geochronological and Lu-Hf Isotopic Constraints on the Precambrian Magmatic and Crustal Evolution of the Western Yangtze Block, SW China. *Precambrian Res.* 172, 99–126. doi:10.1016/j.precamres.2009.03.010

Sun, W., Zhou, M., Yan, D., Li, J., and Ma, Y. (2008). Provenance and Tectonic Setting of the Neoproterozoic Yanbian Group, Western Yangtze Block (SW China). *Precambrian Res.* 167, 213–236. doi:10.1016/j.precamres.2008.08.001

Tapponnier, P., Zhiqin, X., Roger, F., Meyer, B., Arnaud, N., Wittlinger, G., et al. (2001). Oblique Stepwise Rise and Growth of the Tibet Plateau. *Science* 294, 1671–1677. doi:10.1126/science.105978

Tung, K., Yang, H.-J., Yang, H.-Y., Liu, D., Zhang, J., Wan, Y., et al. (2007). SHRIMP U-Pb Geochronology of the Zircons from the Precambrian Basement of the Qilian Block and its Geological Significances. *Chin. Sci Bull* 52, 2687–2701. doi:10.1007/s11434-007-0356-0

Vervoort, J. D., Patchett, P. J., Söderlund, U., and Baker, M. (2004). Isotopic Composition of Yb and the Determination of Lu Concentrations and Lu/Hf Ratios by Isotope Dilution Using MC-ICPMS. *Geochem. Geophys. Geosyst.* 5, a–n. doi:10.1029/2004GC000721

Wang, C., Dai, J., Zhao, X., Li, Y., Graham, S. A., He, D., et al. (2014a). Outward-growth of the Tibetan Plateau during the Cenozoic: A Review. *Tectonophysics* 621, 1–43. doi:10.1016/j.tecto.2014.01.036

Wang, L.-J., Griffin, W. L., Yu, J.-H., and O'Reilly, S. Y. (2013). U-pb and Lu-Hf Isotopes in Detrital Zircon from Neoproterozoic Sedimentary Rocks in the Northern Yangtze Block: Implications for Precambrian Crustal Evolution. *Gondwana Res.* 23, 1261–1272. doi:10.1016/j.gr.2012.04.013

Wang, L.-J., Griffin, W. L., Yu, J.-H., and O'Reilly, S. Y. (2010). Precambrian Crustal Evolution of the Yangtze Block Tracked by Detrital Zircons from Neoproterozoic Sedimentary Rocks. *Precambrian Res.* 177, 131–144. doi:10.1016/j.precamres.2009.11.008

Wang, L.-J., Yu, J.-H., Griffin, W. L., and O'Reilly, S. Y. (2012). Early Crustal Evolution in the Western Yangtze Block: Evidence from U-Pb and Lu-Hf Isotopes on Detrital Zircons from Sedimentary Rocks. *Precambrian Res.* 222-223, 368–385. doi:10.1016/j.precamres.2011.08.001

Wang, W., Zhou, M.-F., Zhao, X.-F., Chen, W.-T., and Yan, D.-P. (2014b). Late Paleoproterozoic to Mesoproterozoic Rift Successions in SW China: Implication for the Yangtze Block-North Australia-Northwest Laurentia Connection in the Columbia Supercontinent. *Sediment. Geology.* 309, 33–47. doi:10.1016/j.sedgeo.2014.05.004

Wang, Z., Wang, J., Deng, Q., Du, Q., Zhou, X., Yang, F., et al. (2015). Paleoproterozoic I-type Granites and Their Implications for the Yangtze Block Position in the Columbia Supercontinent: Evidence from the Lengshui Complex, South China. *Precambrian Res.* 263, 157–173. doi:10.1016/j.precamres.2015.03.014

Wu, C., Gao, Y., Wu, S., Chert, Q. L., Wooden, J. L., Mmdab, F. K., et al. (2007a). Zircon SHRIMP U-Pb Dating of Granites from the Da Qaidam Area in the North Margin of Qaidam Basin. *Acta Petrologica Siniea* 23, 1861–1875. NW Chinain Chinese with English abstract.

Wu, C., Yang, J., Wooden, J., Liou, J., Li, H., and Meng, F. (2001). Zircon SHRIMP Dating of Granite from Qaidam Mountains. *Chin. Sci. Bull.* 46, 1743–1747. in Chinese with English abstract.

Wu, C., Yang, J., Xu, Z., Wooden, J. L., Ireland, T., Li, H., et al. (2004). Granitic Magmatism on the Early Paleozoic UHP Belt of Northern Qaidam, NW China. *Acta Geol. Sin.* 78 (5), 658–674. in Chinese with English abstract.

Wu, F.-Y., Yang, Y.-H., Xie, L.-W., Yang, J.-H., and Xu, P. (2006). Hf Isotopic Compositions of the Standard Zircons and Baddeleyites Used in U-Pb Geochronology. *Chem. Geology.* 234, 105–126. doi:10.1016/j.chemgeo.2006.05.003

Wu, F., Li, X., Zheng, Y., and Gao, S. (2007b). Lu-Hf Isotopic Systematics and Their Applications in Petrology. *Acta Petrol. Sin.* 23, 185–220. in Chinese with English abstract.

Wu, F., Wan, B., Zhao, L., Xiao, W., and Zhu, R. (2020). Tethyan Geodynamics. *Acta Petrol. Sin.* 36, 1627–1674. in Chinese with English abstract. doi:10.1007/s10114-020-9057-2

Wu, S. (2008). *The Petrogenesis of Paleozoic Granitoids in the North Margin of Qaidam Basin and Their Orogenic Response*. Dissertation. Beijing, China: Chinese Academy of Geological Sciences. [in Chinese with English abstract].

Wu, Y., Gao, S., Zhang, H., Zheng, J., Liu, X., Wang, H., et al. (2012). Geochemistry and Zircon U-Pb Geochronology of Paleoproterozoic Arc Related Granitoid in the Northwestern Yangtze Block and its Geological Implications. *Precambrian Res.* 200-203, 26–37. doi:10.1016/j.precamres.2011.12.015

Xiong, F., Ma, C., Zhang, J., Liu, B., and Jiang, H. a. (2014). Reworking of Old continental Lithosphere: an Important Crustal Evolution Mechanism in Orogenic Belts, as Evidenced by Triassic I-type Granitoids in the East Kunlun Orogen, Northern Tibetan Plateau. *J. Geol. Soc.* 171, 847–863. doi:10.1144/jgs2013-038

Xu, W., Zhang, H., and Liu, X. (2007). U-pb Zircon Dating Constraints on Formation Time of Qilian High-Grade Metamorphic Rock and its Tectonic Implications. *Chin. Sci Bull* 52, 531–538. doi:10.1007/s11434-007-0082-7

Xu, Y., Du, Y., and Yang, J. (2013). Tectonic Evolution of the North Qilian Orogenic Belt from the Late Ordovician to Devonian: Evidence from Detrital Zircon Geochronology. *Earth Science-Journal China Univ. Geosciences* 38, 934–946. in Chinese with English abstract.

Xu, Y., Wang, C. Y., and Zhao, T. (2016). Using Detrital Zircons from River Sands to Constrain Major Tectono-Thermal Events of the Cathaysia Block, SE China. *J. Asian Earth Sci.* 124, 1–13. doi:10.1016/j.jseaes.2016.04.012

Yan, Q., Pei, X., Li, R., Li, Z., Pei, L., Liu, C., et al. (2017a). Detrital Zircon U-Pb Age and Geological Significance of Metamorphic Strata at Gouli Area in the Central Tectonic Belt of East Kunlun. *Northwest. Geology.* 50, 165–181. in Chinese with English abstract. doi:10.3799/dqkx.2013.092

Yan, Y., Yang, B., Li, H., Cai, H., Xu, H., and Xu, Y. (2017b). Single-Zircon U-Pb and Geological Significance of Metamorphic and Intrusive System of Nalingele Region in East Kunlun Neo-Proterozoic. *Northwest. Geology.* 50, 33–40. in Chinese with English abstract.

Yang, J., Gao, S., Chen, C., Tang, Y., Yuan, H., Gong, H., et al. (2009). Episodic Crustal Growth of North China as Revealed by U-Pb Age and Hf Isotopes of Detrital Zircons from Modern Rivers. *Geochimica et Cosmochimica Acta* 73, 2660–2673. doi:10.1016/j.gca.2009.02.007

Yin, A., Dang, Y.-Q., Wang, L.-C., Jiang, W.-M., Zhou, S.-P., Chen, X.-H., et al. (2008). Cenozoic Tectonic Evolution of Qaidam basin and its Surrounding Regions (Part 1): The Southern Qilian Shan-Nan Shan Thrust belt and Northern Qaidam basin. *Geol. Soc. America Bull.* 120, 813–846. doi:10.1130/b26180.1

Yin, F., Wang, D., Sun, Z., Ren, G., and Pang, W. (2012). Columbia Supercontinent: New Insights from the Western Margin of the Yangtze Landmass. *Sediment. Geology. Tethyan Geology.* 32, 31–40. in Chinese with English abstract.

Yu, S., Zhang, J., and Hou, K. (2011). Two Constrasting Magmatic Events in the Dulan UHP Metamorphic Terrane: Implication for Collisional Orogeny. *Acta Petrol. Sin.* 27, 3335–3349. in Chinese with English abstract.

Yuan, W., Mo, X., Yu, X., and Luo, Z. (2000). The Record of Indosinian Tectonic Setting from the Granotoid of Eastern Kunlun Mountains. *Geol. Rev.* 46, 203–211. in Chinese with English abstract.

Yusheng, W., Jianxin, Z., Jingsui, Y., and Zhiqin, X. (2006). Geochemistry of High-Grade Metamorphic Rocks of the North Qaidam Mountains and Their Geological Significance. *J. Asian Earth Sci.* 28, 174–184. doi:10.1016/j.jseaes.2005.09.018

Yusheng, W., Zhiqin, X., Jingsui, Y., and Jianxin, Z. (2001). Ages and Compositions of the Precambrian High-Grade Basement of the Qilian Terrane and its Adjacent Areas. *Acta Geol. Sin.-Engl. Ed.* 75, 375–384. doi:10.1111/j.1755-6724.2001.tb00055.x

Zhang, G., Ireland, T., Zhang, L., Gao, Z., and Song, S. (2016). Zircon Geochemistry of Two Contrasting Types of Eclogite: Implications for the Tectonic Evolution of the North Qaidam UHPM Belt, Northern Tibet. *Gondwana Res.* 35, 27–39. doi:10.1016/j.gr.2016.04.002

Zhang, G., Song, S., Zhang, L., Niu, Y., and Shu, G. (2005). Ophiolite-Type Mantle Peridotite from Shaliuhe, North Qaidam UHPM Belt, NW China and its Tectonic Implications. *Acta Petrol. Sin.* 21, 1049–1058. in Chinese with English abstract.

Zhang, G., Song, S., Zhang, L., and Niu, Y. (2008a). The Subducted Oceanic Crust within Continental-Type UHP Metamorphic Belt in the North Qaidam, NW China: Evidence from Petrology, Geochemistry and Geochronology. *Lithos* 104, 99–118. doi:10.1016/j.lithos.2007.12.001

Zhang, G., Zhang, L., and Christy, A. G. (2013). From Oceanic Subduction to continental Collision: An Overview of HP-UHP Metamorphic Rocks in the North Qaidam UHP belt, NW China. *J. Asian Earth Sci.* 63, 98–111. doi:10.1016/j.jseaes.2012.07.014

Zhang, G., Zhang, L., Christy, A. G., Song, S., and Li, Q. (2014). Differential Exhumation and Cooling History of North Qaidam UHP Metamorphic Rocks, NW China: Constraints from Zircon and Rutile Thermometry and U-Pb Geochronology. *Lithos* 205, 15–27. doi:10.1016/j.lithos.2014.06.018

Zhang, G., and Zhang, L. (2011). Rodingite from Oceanic Lithology of Shaliu Terrane in North Qaidam UHPM Belt and its Geological Implication. *Earth Sci. Front.* 18, 151–157. in Chinese with English abstract.

Zhang, G., Zhang, L., Song, S., and Niu, Y. (2009). UHP Metamorphic Evolution and SHRIMP Geochronology of a Coesite-Bearing Meta-Ophiolitic Gabbro in the North Qaidam, NW China. *J. Asian Earth Sci.* 35, 310–322. doi:10.1016/j.jseaes.2008.11.013

Zhang, J., Wan, Y., Meng, F., Yang, J., and Xu, A. (2003). Geochemistry, Sm-Nd and U-Pb Isotope Study of Gneisses (Schists) Enclosing Eclogites in the North Qaidam Mountains - Deeply Subducted Precambrian Metamorphic Basement? *Acta Petrol. Sin.* 19, 443–451. in Chinese with English abstract.

Zhang, J., Yu, S., and Meng, F. (2008b). Metamorphic and Deformational Evolution of the Iqe-Luofengpo Eclogite-Geniss Unit in the North Qaidam Mountains, China. *Geol. Bull. China* 27, 1468–1474. in Chinese with English abstract.

Zhang, S., Jian, X., Pullen, A., Fu, L., Liang, H., Hong, D., et al. (2020). Tectono-Magmatic Events of the Qilian Orogenic Belt in Northern Tibet: New Insights

from Detrital Zircon Geochronology of River Sands. *Int. Geology. Rev.* 63, 917–940. doi:10.1080/00206814.2020.1734876

Zhou, C.-A., Song, S., Allen, M. B., Wang, C., Su, L., and Wang, M. (2021). Post-collisional Mafic Magmatism: Insights into Orogenic Collapse and Mantle Modification from North Qaidam Collisional Belt, NW China. *Lithos* 398-399, 106311. doi:10.1016/j.lithos.2021.106311

Zhu, Z., Campbell, I. H., Allen, C. M., and Burnham, A. D. (2020). S-type Granites: Their Origin and Distribution through Time as Determined from Detrital Zircons. *Earth Planet. Sci. LettersSci. Lett.* 536, 116140. doi:10.1016/j.epsl.2020.116140

**Conflict of Interest:** The authors declare that the research was conducted in the absence of any commercial or financial relationships that could be construed as a potential conflict of interest.

**Publisher's Note:** All claims expressed in this article are solely those of the authors and do not necessarily represent those of their affiliated organizations, or those of the publisher, the editors and the reviewers. Any product that may be evaluated in this article, or claim that may be made by its manufacturer, is not guaranteed or endorsed by the publisher.